Southern Ocean calcification controls the global distribution of alkalinity

Kristen Marie Krumhardt[1], Matthew C. Long[2], Keith Lindsay[2], and Michael N Levy[2]

[1]National Center for Atmospheric Research
[2]National Center for Atmospheric Research (UCAR)

November 24, 2022

Abstract

Biological processes in Southern Ocean surface waters have widespread impacts on global productivity and oceanic CO2 storage. Here, we demonstrate that biological calcification in the Southern Ocean exerts a strong control the global distribution of alkalinity. The signature of Southern Ocean calcification is evident in observations as a depletion of potential alkalinity within portions of Subantarctic Mode and Intermediate water. Experiments with an ocean general circulation model indicate that calcification and subsequent sinking of biogenic carbonate in this region effectively transfers alkalinity between the upper and lower cells of the meridional overturning circulation. Southern Ocean calcification traps alkalinity in the deep ocean; decreasing calcification permits more alkalinity to leak out from the Southern Ocean, yielding increased alkalinity in the upper cell and low-latitude surface waters. These processes have implications for the atmosphere-ocean partitioning of carbon. Reductions in Southern Ocean calcification increase the buffer capacity of surface waters globally, thereby enhancing the ocean's ability to absorb carbon from the atmosphere. This study highlights the critical role of Southern Ocean calcification in determining global alkalinity distributions, demonstrating that changes in this process have the potential for widespread consequences impacting air-sea partitioning of CO2.

Southern Ocean calcification controls the global distribution of alkalinity

K. M. Krumhardt[1], M. C. Long[1], K. Lindsay[1], M. N. Levy[1]

[1]Climate and Global Dynamics, National Center for Atmospheric Research, Boulder, Colorado, U.S.A.

Key Points:

- Calcification in the Southern Ocean affects the global distribution of alkalinity
- Changes in Southern Ocean calcification affect how the ocean absorbs atmospheric carbon dioxide
- Southern Ocean calcium carbonate fluxes control the strength of the Southern Ocean alkalinity trap

Corresponding author: Kristen M. Krumhardt, kristenk@ucar.edu

Abstract

Biological processes in Southern Ocean surface waters have widespread impacts on global productivity and oceanic CO_2 storage. Here, we demonstrate that biological calcification in the Southern Ocean exerts a strong control the global distribution of alkalinity. The signature of Southern Ocean calcification is evident in observations as a depletion of potential alkalinity within portions of Subantarctic Mode and Intermediate water. Experiments with an ocean general circulation model indicate that calcification and subsequent sinking of biogenic carbonate in this region effectively transfers alkalinity between the upper and lower cells of the meridional overturning circulation. Southern Ocean calcification traps alkalinity in the deep ocean; decreasing calcification permits more alkalinity to leak out from the Southern Ocean, yielding increased alkalinity in the upper cell and low-latitude surface waters. These processes have implications for the atmosphere-ocean partitioning of carbon. Reductions in Southern Ocean calcification increase the buffer capacity of surface waters globally, thereby enhancing the ocean's ability to absorb carbon from the atmosphere. This study highlights the critical role of Southern Ocean calcification in determining global alkalinity distributions, demonstrating that changes in this process have the potential for widespread consequences impacting air-sea partitioning of CO_2.

Plain Language Summary

Plankton living in the Southern Ocean affect the composition of seawater through biological processes. Due to the particular oceanic circulation in the Southern Ocean, these biologically-driven changes in ocean chemistry can have widespread effects on the global ocean. Species of plankton that form shells of calcium carbonate remove alkalinity from surface waters through the process of calcification. The amount of alkalinity in surface waters is important because it affects how much CO_2 the ocean can absorb from the atmosphere. We show that Southern Ocean calcifying plankton affect the global distribution of alkalinity through the presence of a Southern Ocean "alkalinity trap." More Southern Ocean calcification yields a stronger alkalinity trap, with more alkalinity being retained in the Southern Ocean and in deep waters, away from the atmosphere. Reduced calcification in the Southern Ocean permits more alkalinity to escape the Southern Ocean and remain in the upper ocean globally. These changes affect oceanic CO_2 uptake from the atmosphere.

1 Introduction

The Southern Ocean is uniquely important to the climate system and global biogeochemistry because it is a dominant region for ventilation of the deep ocean. The biological pump deposits nutrients at depth; circulation must ultimately provide a path to return nutrients to the ocean surface, otherwise productivity would cease. The nature of nutrient return paths is important as it determines the degree to which global ocean biogeochemistry is sensitive to climate. W. S. Broecker (1991) envisioned that nutrients were mixed across the main thermocline ubiquitously in the global ocean; this model, however, is inconsistent with observed vertical diffusivities, which are about an order of magnitude too low to account for the necessary water mass transformations (Ledwell et al., 1993). A more accurate account of nutrient return paths is that deep ocean nutrients are returned to the surface in the Southern Ocean by the global overturning circulation (Sarmiento et al., 2007). In the Southern Ocean upwelled nutrients are exposed to productivity before being returned to the subtropical thermocline in Antarctic Intermediate (AAIW) and Subantarctic Mode Water (SAMW)—or the abyssal ocean in Antarctic Bottom Water (AABW) (Figure 1). As a result, biological processes occurring in Southern Ocean surface waters have the capacity to influence global productivity and biogeochemistry (Sarmiento et al., 2004; Marinov et al., 2006).

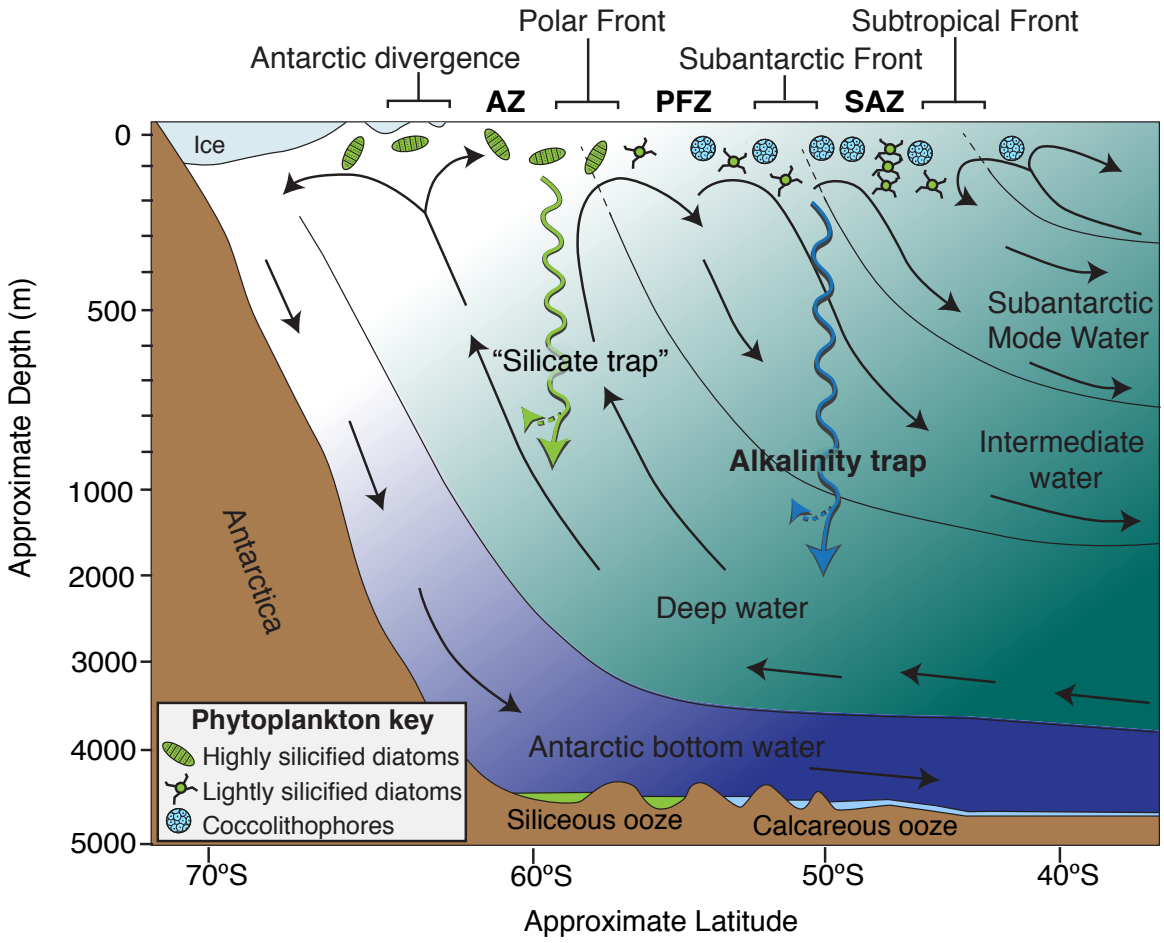

Figure 1. Schematic of idealized, zonal-mean Southern Ocean overturning circulation, showing dominant biomineralizing phytoplankton. Abbreviations: AZ = Antarctic zone; PFZ = Polar front zone; SAZ = Subantarctic zone.

Latitudinal gradients in nutrients and temperature define unique environments in the Southern Ocean and impact plankton assemblages and their physiological state, which, in turn, may affect water chemistry. For example, strong iron limitation in the silicate (SiO_3)-rich waters of Antarctic zone (AZ; Figure 1) of the Southern Ocean is conducive to the production of heavily silicified diatoms (Assmy et al., 2013; Franck et al., 2000; Leynaert et al., 2004; Smith et al., 2017). These diatoms deplete silicic acid in the surface waters to build thick, grazer-resistant, opal shells, which sink and leave less SiO_3 to be distributed to the rest of the ocean as waters move north (Sarmiento et al., 2004; Assmy et al., 2013). In contrast, the Subantarctic zone (SAZ; Figure 1) is characterized by limiting SiO_3, more plentiful iron input, and warmer temperatures; these conditions create a region of competition between calcifying phytoplankton, i.e., coccolithophores, (Balch et al., 2016) and lightly silicified diatoms (Assmy et al., 2013; Tréguer et al., 2018; Smith et al., 2017). These distinct Southern Ocean plankton communities are reflected in the composition of material found in sediment traps (Figure 2a; Rembauville et al., 2016; Wilks et al., 2017; Honjo et al., 2000) and seafloor sediments (Figure 2b; Dutkiewicz et al., 2015). Due to differing cellular stoichiometry and physiology, these Southern Ocean plankton communities leave unique impressions on water masses and contribute to an ecological divide between the AZ and SAZ (e.g., Malinverno et al., 2016).

Several studies have explored the effect of Southern Ocean phytoplankton production on global nutrient distributions (Sarmiento et al., 2004; Marinov et al., 2006; Primeau et al., 2013; Sarmiento et al., 2004; Dutkiewicz et al., 2005). In particular, a phenomenon known as Southern Ocean "nutrient trapping" is considered a mechanism that might drive reorganizations of the global nutrient inventory distribution (Primeau et al., 2013; Moore et al., 2018). Nutrient trapping is possible in regions with divergent flow at the surface and convergent flow at depth; in this case, upwelled nutrients fuel export production, but sinking organic material rains back down and is remineralized at the same depths from which the upwelled water mass came. Nutrients can be effectively trapped if export production is fast relative to the timescale at which advection flushes the region; where this is true, nutrients are trapped, increasing concentrations locally and limiting lateral transport out of the region. Primeau et al. (2013) demonstrated in the context of an ocean general circulation (OGCM) that nutrients can be most effectively trapped in the Southern Ocean by increasing productivity in the Antarctic Zone. This phenomenon was simulated in Earth system model (ESM) integrations conducted out to year 2300 with continuing carbon emission (Moore et al., 2018).

Nutrient trapping already manifests in the Southern Ocean and involves decoupling between the macronutrients silicic acid and nitrate (Sarmiento et al., 2004). Diatoms typically utilize silicic acid and nitrate in a ratio of about 1:1 under adequate light and nutrient conditions. However, as alluded to above, stress induced by light or iron scarcity causes diatoms to increase their Si:N utilization ratio (e.g., Takeda, 1998). As a result of elevated Si:N utilization in the Southern Ocean, silicic acid is preferentially removed as waters upwelled at the APF flow northward to the subduction regions north of the SAF, where AAIW and SAMW are formed ("Silicate trap" on Figure 1). Sarmiento et al. (2004) showed that diatom opal formation in the Southern Ocean limits the amount of SiO_3 that leaves the Southern Ocean, thereby influencing diatom production in the rest of the Southern hemisphere and North Atlantic via SAMW. Another dominant surface process in the formation region of these waters is calcification, which is especially widespread in the SAZ and PFZ of the Southern Ocean (Figures 1 and 2; Balch et al., 2011; Salter et al., 2014). The potential effect of Southern Ocean calcification on global alkalinity distributions has received limited attention.

Calcification impacts seawater alkalinity and, in turn, affects air-sea CO_2 fluxes. Producing one mole of $CaCO_3$ removes two moles of alkalinity and one mole of dissolved inorganic carbon (DIC) from ambient seawater (Sarmiento & Gruber, 2006). Sinking $CaCO_3$ transfers carbon to depth, creating the "carbonate pump," but consumption of alkalin-

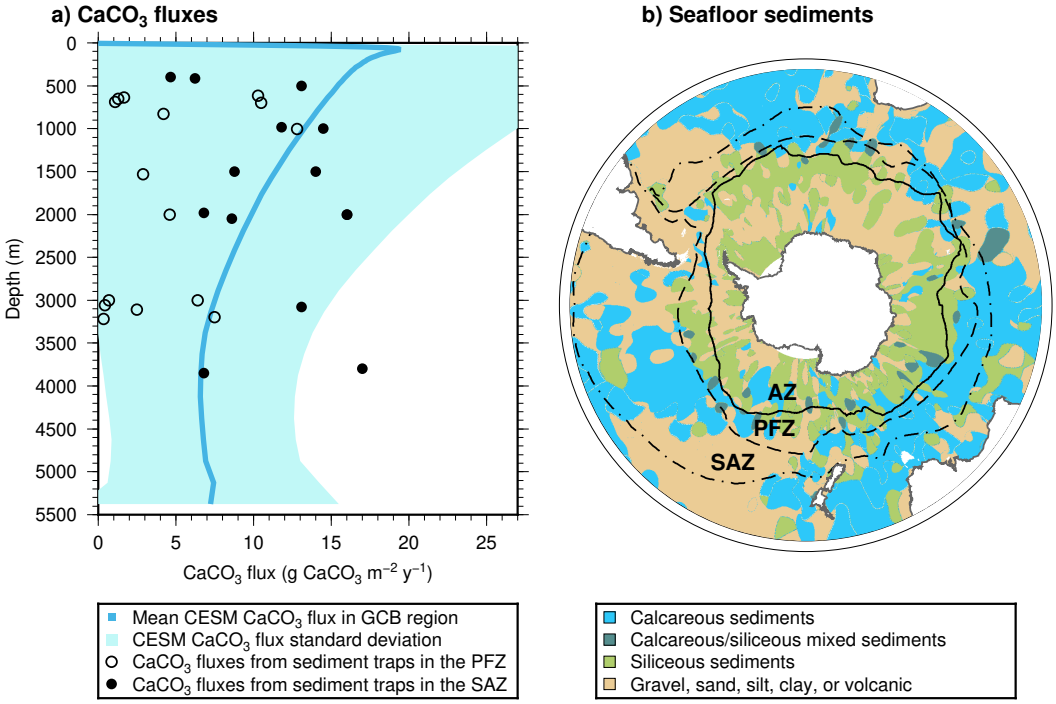

Figure 2. $CaCO_3$ in the water column and on the seafloor. Panel (a) shows $CaCO_3$ fluxes from sediment traps moored in the SAZ (filled circles) and PFZ (open circles) of the Southern Ocean and $CaCO_3$ fluxes from the Community Earth System Model (CESM). Data sources for $CaCO_3$ fluxes from sediment traps and sediment grouping specifications are described in Section 2.1. The CESM $CaCO_3$ fluxes are an area-weighted mean underneath the $26.0 \leq \sigma_\theta \leq 27.0$ outcrop region (darker blue line) with the standard deviation of fluxes within this region indicated by the light blue shading. (b) Seafloor sediments from Dutkiewicz et al. (2015). Fronts shown on panel (b) are, from south to north, the Polar Front (Freeman & Lovenduski, 2016), the Subantarctic Front and the Subtropical Front (Orsi et al., 1995). Abbreviations: AZ = Antarctic zone; PFZ = Polar front zone; SAZ = Subantarctic zone.

ity at the ocean surface diminishes the ocean's ability to absorb CO_2 from the atmosphere relative to a pure "soft-tissue" pump (e.g., Salter et al., 2014). Hence the ratio of $CaCO_3$ to particulate organic carbon (POC) flux, the rain ratio, is an important metric of the efficacy of the biological pump (e.g., Sigman et al., 2010; Sarmiento et al., 2002). Matsumoto et al. (2002), for instance, used a simple box model to show that changes in the rain ratio can impact ocean carbon storage; by increasing diatom production in the global ocean at the expense of coccolithophores, they diminished the rain ratio, driving decreases in atmospheric CO_2 via enhanced ocean carbon storage. This, and many other studies, have highlighted the importance of surface ocean alkalinity on CO_2 uptake and climate.

The Southern Ocean is home to the Great Calcite Belt (GCB; Balch et al., 2011), a circumpolar band of elevated particulate inorganic carbon (PIC) that is visible from space due to the high reflectivity of suspended $CaCO_3$ (Balch et al., 2011; Holligan et al., 2010). While there are multiple calcifying organisms in the GCB region (the SAZ and PFZ), the PIC algorithm that translates water-leaving radiances and backscattering to $CaCO_3$ concentrations is primarily tuned to capture coccolithophore shells (Gordon et al., 2001; Balch et al., 2005). Coccolithophore blooms in the Southern Ocean are extensive, covering $\sim$52 x 10^6 km^2 and accounting for roughly 26% of oceanic suspended PIC (Balch et al., 2005). Indeed, coccolithophores are a large driver of $CaCO_3$ fluxes in the SAZ, with contributions ranging from $\sim$10% to >85% of total $CaCO_3$ (Wilks et al., 2017; Rigual Hernández et al., 2020; Manno et al., 2018; Rembauville et al., 2016). Zooplankton calcifiers, pteropods and foraminifera, also constitute significant portions of $CaCO_3$ fluxes in the Southern Ocean (Rigual Hernández et al., 2018; Hunt et al., 2008). For example, Manno et al. (2018) showed that pteropods comprise the majority of $CaCO_3$ fluxes (in the more soluble form, aragonite) during the autumn between 1500 m and 2000 m of depth at two sites in the SAZ. A global biogeochemical model recently showed that pteropods contribute largely to shallow $CaCO_3$ export globally (Buitenhuis et al., 2019), while coccolithophores and foraminifera dominate deep fluxes to sediments (W. Broecker & Clark, 2009). Figure 2a shows total $CaCO_3$ collected in sediment traps moored in the GCB region of the Southern Ocean, indicating that sinking biogenic $CaCO_3$ reaches deeper than 2000 m with low dissolution. At this depth, deep waters are moving south (Talley et al., 2003), setting up the potential for Southern Ocean alkalinity trapping (Figure 1).

Observational studies have established direct links between surface alkalinity and local $CaCO_3$ formation and dissolution. For example, decreases in surface alkalinity resulting from biological calcification have been documented in subtropical and subpolar North Atlantic (Bates et al., 1996; Holligan et al., 1993; Robertson et al., 1994), as well as the Southern Ocean (Balch et al., 2016). Conversely, Cross et al. (2013) observed increases in total alkalinity associated with $CaCO_3$ dissolution in corrosive waters of the North Pacific. In addition to $CaCO_3$ cycling, alkalinity is affected by freshwater fluxes and the production of organic matter through nitrate consumption. To isolate the impact of $CaCO_3$ cycling, we make use of "potential alkalinity (sPAlk)," which is a linear combination of alkalinity and nitrate, normalized to a reference salinity (Sarmiento & Gruber, 2006). Fry et al. (2015) used sPAlk as a basis for a tracer they called Alk*, from which riverine influences on alkalinity have also been removed. Alk* is remarkably consistent throughout low latitudes in all ocean basins, but increases in the North Pacific and high-latitude Southern Ocean (Fry et al., 2015; Millero et al., 1998), reminiscent of SiO_3 distributions (Levitus et al., 1993; Freeman et al., 2018). Alk* declines in SAZ surface waters moving north at $\sim$40°S, a region rich in coccolithophores and other pelagic calcifiers. Jin et al. (2006) diagnosed $CaCO_3$ production globally by restoring sPAlk to observations within an ocean general circulation model, finding that Southern Ocean calcification accounts for more than one third of global oceanic calcification. In summary, there is widespread calcification in the Southern Ocean that likely imprints on ocean chemistry downstream from the Southern Ocean environment.

Given the physical dynamics of the Southern Ocean, changes in calcification in the Southern Ocean could have widespread biogeochemical consequences. In this study, we test the hypothesis that Southern Ocean calcification is modifying global alkalinity distributions. We first present observational evidence that $CaCO_3$ production in the Southern Ocean leaves a signature on alkalinity concentrations and could lead to "alkalinity trapping" in the Southern Ocean, as has been shown for silicate, other macronutrients, and carbon (e.g., Primeau et al., 2013; Sarmiento et al., 2004; Marinov et al., 2006). We then use an ocean general circulation model coupled to a biogeochemistry model to quantify the effects of Southern Ocean calcification on the global distribution of alkalinity. Our results show that calcification in the GCB region of the Southern Ocean modifies global alkalinity by limiting the amount of alkalinity that flows northward in the upper water column of the Subantarctic Southern Ocean. Changing Southern Ocean calcification redistributes ocean alkalinity between upper and lower cells of the overturning circulation and between the Southern Ocean and the rest of the global ocean. This has consequences on biogeochemical processes, such as global air-sea CO_2 fluxes. The results of our model sensitivity tests show that changes in calcification in the GCB region could have widespread impacts beyond the Southern Ocean and alter the overall amount of carbon that the ocean absorbs from the atmosphere globally.

2 Methods

2.1 Observational datasets

We used GLODAP version 2 (Lauvset et al., 2016) to examine observational evidence of Southern Ocean calcification on alkalinity. By removing the influences of precipitation, evaporation, and the production and remineralization of organic matter on alkalinity distributions, salinity-normalized potential alkalinity (sPAlk) helps to isolate the effects of $CaCO_3$ production and dissolution on alkalinity. We calculated sPAlk following Fry et al. (2015):

$$sPAlk = (Alk + 1.36 \times \mathrm{NO_3})\frac{35}{S} \tag{1}$$

where Alk is the total alkalinity concentration, NO_3 is the nitrate concentration, and S is the salinity. The factor of 1.36 accounts for the average proportional uptake of other ions consumed by primary production, such as phosphate and sulfate (Wolf-Gladrow et al., 2007). We interpolated $sPAlk$ onto σ_θ density coordinates to examine the climatological mean fields within isopycnal density ranges. We compute $sPAlk$ on output from a numerical model similarly; however, we do not apply salinity normalization to the simulated NO_3, as freshwater fluxes are not applied to NO_3 in the model.

We used satellite-derived particulate inorganic carbon (PIC) from MODIS (Balch et al., 2005; Gordon et al., 2001) to assess the location of the Great Calcite Belt (GCB), generating an annual mean PIC map for the period 2003 to 2017. We compare these to $CaCO_3$ concentrations simulated in the top level of the ocean model (see Section 2.2), which represents the upper 10 m.

We compiled $CaCO_3$ flux data from sediment traps moored in the SAZ (between the subtropical front and Subantarctic front) and PFZ (between the Subantarctic front and the Polar Front) in the Southern Ocean. Data on $CaCO_3$ fluxes from sediment traps are from Rigual Hernández et al. (2020), Wilks et al. (2017), Trull et al. (2001), Salter et al. (2014), Northcote and Neil (2005), Wefer and Fischer (1991), Fischer et al. (2002), Manno et al. (2018), and Honjo et al. (2000). We compare this observational $CaCO_3$ flux dataset to modeled $CaCO_3$ fluxes in the Southern Ocean between the 26.0 to 27.0 σ_θ isopycnal surface outcrops.

We use ocean sediment data from Dutkiewicz et al. (2015) to demonstrate the ecological divide between calcifiers and silicifiers in the Southern Ocean. Sediment fields were aggregated to distinguish between siliceous, calcareous, mixed siliceous/calcareous, and

other types of sediments. Siliceous sediments included radiolarian ooze, siliceous ooze, and siliceous mud. Calcareous sediments included calcareous ooze, shells/corals, and fine-grained calcareous sediments.

2.2 Modeling experiments

We use a pre-release version of the Community Earth System Model (CESM) version 2.2 with biogeochemistry to test the effects of Southern Ocean calcification on alkalinity and air-sea CO_2 fluxes. The ocean ecosystem is simulated using the Marine Biogeochemical Library (MARBL; marbl-ecosys.github.io). Our simulations with MARBL include an explicit coccolithophore phytoplankton functional type (PFT; Krumhardt et al., 2019). The coccolithophore PFT parameterization is based on physiological studies, where the ratio of $CaCO_3$ production to photosynthesis in the PFT responds to environmental conditions (temperature, nutrients, and CO_2 concentration). In this study, however, we used an updated relationship between $CaCO_3$ production and temperature (see Figure S1) in order to better fit physiological studies specifically with the Southern Ocean *Emiliania huxleyi* morphotype. We were also guided by comparisons with the simulated satellite observation of surface PIC concentrations in the Southern Ocean (section 2.1).

MARBL only represents phytoplankton calcification; zooplankton calcifiers, such as pteropods and foraminifera, are not simulated. Additionally, the model assumes that all $CaCO_3$ is produced as calcite, thus ignoring the distinction between the mineral forms calcite and aragonite, which may be important in modulating dissolution depths (Gangstø et al., 2008). Despite these details, CESM $CaCO_3$ fluxes in the Southern Ocean compare reasonably well to total $CaCO_3$ fluxes observed in sediment traps (Figure 2). Particulate $CaCO_3$ sinking and dissolution is parameterized according to the formulation of Armstrong et al. (2002) with a reference dissolution length scale of 500 m that does not depend on the $CaCO_3$ saturation state (Ω). The $CaCO_3$ dissolution length scale (as well as POC and SiO_3 dissolution length scales) increases with depth and under low oxygen conditions. Burial of $CaCO_3$ on the ocean floor occurs where $\Omega > \Omega_{crit}$ in the model's bottom layer; where $\Omega < \Omega_{crit}$, all $CaCO_3$ reaching the model's bottom layer is dissolved. In the simulations presented here, Ω_{crit} was set to a value of 1. Riverine nutrient, carbon, and alkalinity fluxes are supplied to the ocean model from a dataset derived from GlobalNEWS (Mayorga et al., 2010). Riverine DIC inputs are assumed to be comprised of 100% bicarbonate and are thus equal to alkalinity fluxes.

MARBL simulates two parallel carbonate systems (i.e., the prognostic DIC and Alk tracers as well as associated diagnostic quantities like pCO_2, pH, etc.). In climate-projection integrations, these tracer systems are identical, except for their atmospheric CO_2 boundary conditions, thus enabling a straightforward characterization of anthropogenic CO_2 distributions inclusive of physical and biogeochemical (i.e., Revelle Factor) feedbacks. We exploited this capability, using the second carbonate-system (ALT_CO2) tracers to examine the impacts of Southern Ocean calcification on alkalinity, DIC, and air-sea CO_2 exchanges. Our approach was to manipulate the $CaCO_3$ production and dissolution terms for the ALT_CO2 tracers in the region south of 30°S. Since all other source/sink terms, atmospheric boundary conditions and physical transport fields for the primary DIC/Alk and ALT_CO2 tracers were identical, this methodology provides a very clean approach to isolating the influence of $CaCO_3$ production and dissolution in the Southern Ocean on alkalinity and carbon fields globally. Our hypothesis was that vertical fluxes of $CaCO_3$ in the Southern Ocean effect an alkalinity transfer that determines the degree to which alkalinity is "trapped" in the region. We approach this in two ways, first by directly manipulating $CaCO_3$ production in the surface ocean south of 30°S and second, by modifying the dissolution length-scales (DLS) south of 30°S, thereby affecting the vertical distribution of dissolution for a given $CaCO_3$ production. In the first case, where we manipulate surface $CaCO_3$ production, the dissolution profile of $CaCO_3$ is impacted in di-

rect proportion to changes in production; the MARBL formulation for $CaCO_3$ cycling requires that the column integrals of production, dissolution and burial sum to zero at each numerical timestep. We ran sensitivity experiments yielding simulated DIC and Alk distributions consistent with five different conditions (Table 1). Our experiments induced only minor changes in $CaCO_3$ burial, leading to very slight differences in total oceanic alkalinity inventory between experiments ($< 0.1\%$; Table 1).

We used an ocean-sea-ice configuration of CESM similar to that described in Long et al. (2013) and Yeager et al. (2018). Ocean physics were spun up for 124 years before simulating ocean biogeochemistry. The CESM sea-ice and ocean component models (with biogeochemistry) were then integrated at the nominal 1-degree resolution for five Coordinated Ocean-Ice Reference Experiment, interannual forcing (CORE-IAF; Large & Yeager, 2009) cycles (62 years/cycle) under preindustrial conditions (atmospheric CO_2 = 284.7 μatm) for a total of 310 years. While this is not long enough to achieve equilibrium with respect to deep ocean alkalinity distributions (which takes thousands of years), is does enable evaluating the dominant patterns of change associated with perturbing Southern Ocean calcification and its impact on alkalinity redistribution.

2.3 Analysis

We focus our analysis on the mean fields over the last 62-year CORE-IAF cycle (simulation years 249–310). Our primary method of evaluating the importance of Southern Ocean calcification is to difference fields in each sensitivity experiment from the control integration; we use this approach to develop a relationship between $CaCO_3$ fluxes in the GCB region of the Southern Ocean and mean alkalinity in the upper ocean. We examine the redistribution of the alkalinity inventory in each experiment using $\sigma_\theta = 27.4$ as the boundary between the upper and lower ocean. In order to better understand the capacity of the ocean to absorb CO_2 from the atmosphere we calculated the Revelle factor. The Revelle factor (R) was estimated by the equation from Sarmiento and Gruber (2006):

$$R = \frac{3 * Alk * DIC - 2 * DIC^2}{(2 * DIC - Alk)(Alk - DIC)} \tag{2}$$

3 Results

3.1 CESM simulation of Southern Ocean calcification

We compare the mean particulate inorganic carbon (PIC) inferred from MODIS (mean 2003-2017) and CESM surface $CaCO_3$ (Figure 3a,b). While CESM simulates a GCB, as in the observational estimates, it tends to be more concentrated and extends somewhat farther north than the PIC observational estimates suggest. It has been noted in several studies that the PIC algorithm likely overestimates PIC in the Southern Ocean, particularly in the AZ (e.g., see Balch et al., 2016; Trull et al., 2018). The coccolithophore PFT is the only source of biogenic $CaCO_3$ in CESM. Therefore, it implicitly represents all pelagic calcification (by zooplankton and phytoplankton) in a biogeochemical sense. Considering this model simplification, an overestimation of coccolithophore $CaCO_3$ (Figure 3b) helps to compensate for the lack of zooplankton calcifiers in the model. Indeed, simulated sinking $CaCO_3$ fluxes compare reasonably well with those derived from sediment traps in the SAZ and PFZ (Figure 2a).

3.2 The signature of calcification in alkalinity observations

We examined salinity-normalized potential alkalinity (sPAlk) in observationally-based fields for a signature of Southern Ocean calcification. In Figure 3c we present the observationally-based estimates of mean sPAlk averaged over the σ_θ isopycnal density range 26.0 and 27.0, which includes SAMW and some portion of AAIW. As waters flow

Table 1. Numerical experiments conducted with the ocean component of the Community Earth System Model (CESM). All metrics are computed as means over the fifth cycle of the CORE-IAF forcing (simulation years 249–310), except for the DIC and Alk accumulation rates, which are the trends over the last two IAF cycles (simulation years 187–310). Abbreviations: DIC = Dissolved Inorganic Carbon; Alk = Alkalinity; DLS = Dissolution Length Scale.

Short name	**Description**	**GCB $CaCO_3$ flux (g $CaCO_3$ m^{-2} yr^{-1})**	**Global mean rain ratio**	**Alk inventory in Pmol (% Δ control)**	**DIC inventory in Pmol (% Δ control)**	**Air-sea CO_2 flux (Pg yr^{-1})**	**DIC accumulation rate (Tmol C yr^{-1})**	**Alk accumulation rate (Tmol Alk yr^{-1})**
control	Standard SO calcification, 500 m DLS	12.91	0.15	3208.92	3056.36	-0.14	23	-0.3
noGCB	No calcification south of 30°S, 500 m DLS	0	0.11	3211.86 (+0.09%)	3060.66 (+0.14%)	-0.24	37	9.7
2xGCB	Double calcification south of 30°S, 500 m DLS	25.82	0.19	3205.98 (-0.09%)	3052.03 (-0.14%)	-0.04	9.2	-10.4
100mDLS	Standard SO calcification, 100 m DLS	3.21	0.13	3210.65 (+0.05%)	3059.00 (+0.09%)	-0.21	32	5.6
1000mDLS	Standard SO calcification, 1000 m DLS	16.71	0.15	3207.77 (-0.04%)	3055.07 (-0.04%)	-0.11	18	-4.6

manuscript submitted to *Global Biogeochemical Cycles*

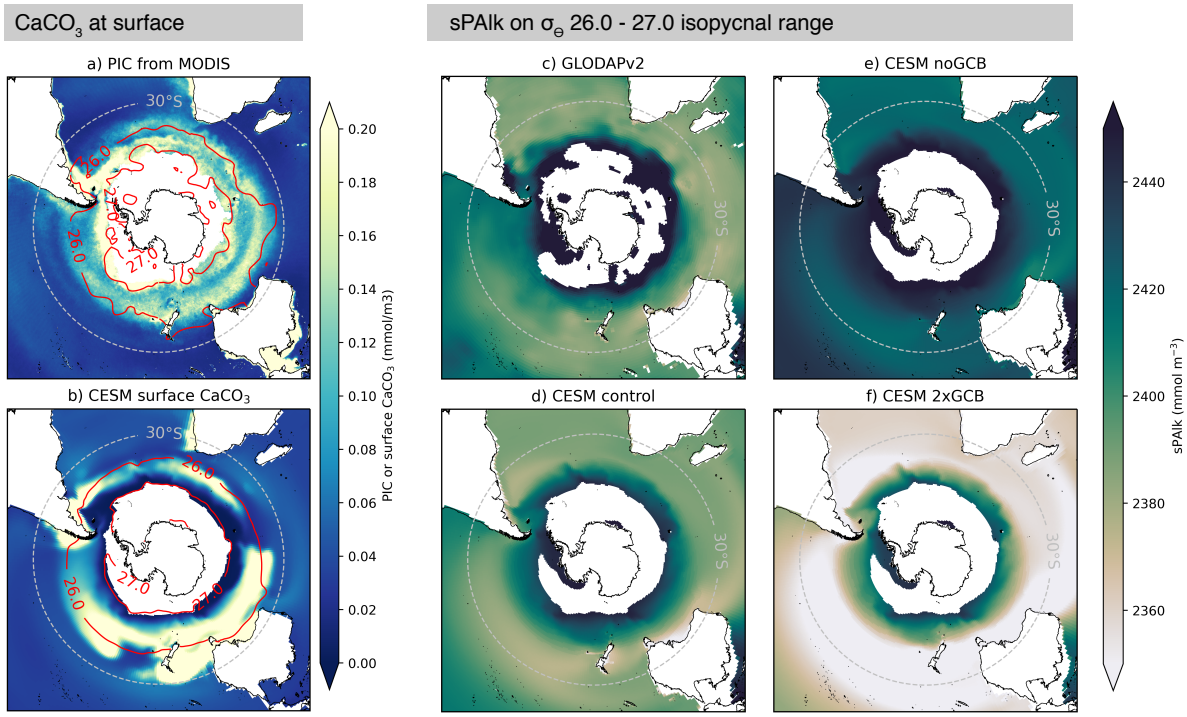

Figure 3. Suspended surface $CaCO_3$ and salinity-normalized potential alkalinity (sPAlk) in observations and CESM. (a) mean annual Particulate Inorganic Carbon (PIC) from MODIS, averaged over the period 2003–2017. Areas where annual mean sea surface temperature is less than 2°C are masked, due to a known temperature range limit of coccolithophores (Holligan et al., 2010) and the unreliability of PIC data near Antarctica (Balch et al., 2016; Trull et al., 2018). (b) Coccolithophore $CaCO_3$ from the CESM at the top level of the ocean model (0–10 m), also masked at 2°C annual mean temperature. Isopycnal outcrop surfaces for σ_θ 26.0 and 27.0 are shown by red contours. (c–f) sPAlk averaged within the σ_θ 26.0 and 27.0 isopycnal range from observations: (c) GLODAP v2; (d) the CESM control; (e) the noGCB experiment; and (f) the 2xGCB experiment. Surface $CaCO_3$ (panel b) and sPAlk from the CESM control and experiments (panels d–f) are averaged over the fifth IAF cycle (years 249–310).

northward from the AZ to the SAZ, sPALK within this density range drops from $> \sim$2450 mmol m^{-3} in the AZ to $\sim$2385 mmol mm^{-3} in the SAZ. Simulated sPAlk from the CESM control simulation shows a similar decline in sPAlk from south to north in this density range (Figure 3d). Modifying Southern Ocean calcification significantly alters the sPAlk distributions relative to the control simulation. Turning calcification off (noGCB) yields a sPAlk field with much smaller declines from the AZ to the SAZ (Figure 3e), which is inconsistent with the pattern in the observations. In contrast, doubling Southern Ocean calcification (2xGCB) yields a reduction in sPAlk (to about $\sim$2365 mmol m^{-3}) that is much larger than the decline evident in the observations (Figure 3f). This comparison demonstrates that sPAlk in the SAMW density range is sensitive to calcification in the GCB region and the annulus of low sPAlk in observations (Figure 3c) is likely attributable to calcification in the SAZ and PFZ of the Southern Ocean. In the following, we explore the widespread impacts of Southern Ocean calcification by analyzing our experimental CESM tracers compared to the control Southern Ocean calcification shown in Figure 3b.

3.3 The impact of Southern Ocean calcification on global alkalinity distributions

Eliminating calcification south of 30°S (noGCB) yields an accumulation of alkalinity in the upper ocean relative to the control (Figure 4a–d). Doubling Southern Ocean calcification shows the opposite effects (Figure 4e–h). Since there is no production of $CaCO_3$ south of 30°S in the noGCB experiment, there is also no dissolution at depth in this region; curtailing this vertical transfer results in a deep ocean alkalinity deficit of $\sim$40 mmol m^{-3} relative to the control concentrated immediately beneath the GCB region (Figure 4a). The deficit is especially strong in the Atlantic and Indian sectors of the Southern Ocean, and somewhat weaker in the Pacific (Figure 4b-d). Again, doubling Southern Ocean calcification (2xGBC) shows precisely the opposite effect (Figure 4e-h). Integrating alkalinity vertically shows that Southern Ocean calcification controls the horizontal transfer of alkalinity from the Southern Ocean to the rest of the ocean (Figure 5). The simulations show especially large sensitivity of the vertically-integrated alkalinity response ($\sim$80 mol m^{-2}) in the North Atlantic (Figure 5). Alkalinity anomalies are transported northward and propagate to depth via the formation of North Atlantic Deepwater (NADW; Figure 4c).

It is important to note that the patterns simulated here do not represent a fully equilibrated state, as there is drift in DIC and Alk inventories (Table 1; Figure S2), as well as in the partitioning of alkalinity vertically in the water column (Figures S3 and S4). The global inventory of alkalinity in each experiment changes in response to a net imbalance between riverine inputs and burial at the sea floor. The global alkalinity inventory in the control simulation happens to be relatively well-balanced, such that the global drift is modest (Table 1). Changing Southern Ocean calcification changes the distribution of Ω and the quantity of $CaCO_3$ incident on the seafloor; reductions in GCB calcification produce a decline in the global $CaCO_3$ burial and, hence, net accumulation of alkalinity in the ocean (Table 1; Figure S2). Since the model buries $CaCO_3$ based on an Ω threshold, the alkalinity inventory will eventually stabilize as alkalinity accumulations drive Ω increases on the sea floor and burial increases to bring the inventory back into balance. We estimate, however, that this adjustment requires $\mathcal{O}(10^4)$ years of integration and is thus not computationally feasible via a brute-force approach. The global drift in alkalinity, however, is quite small relative to the repartitioning of the inventory between upper and low overturning cells, thus it does not ultimately impact our conclusions substantially.

In spite of the complications associated with model drift, these experiments clearly demonstrate that calcification and subsequent vertical transfer of alkalinity in the Subantarctic provides a means of alkalinity trapping. Calcification in the Southern Ocean removes alkalinity from northward flowing waters, transporting it vertically as sinking

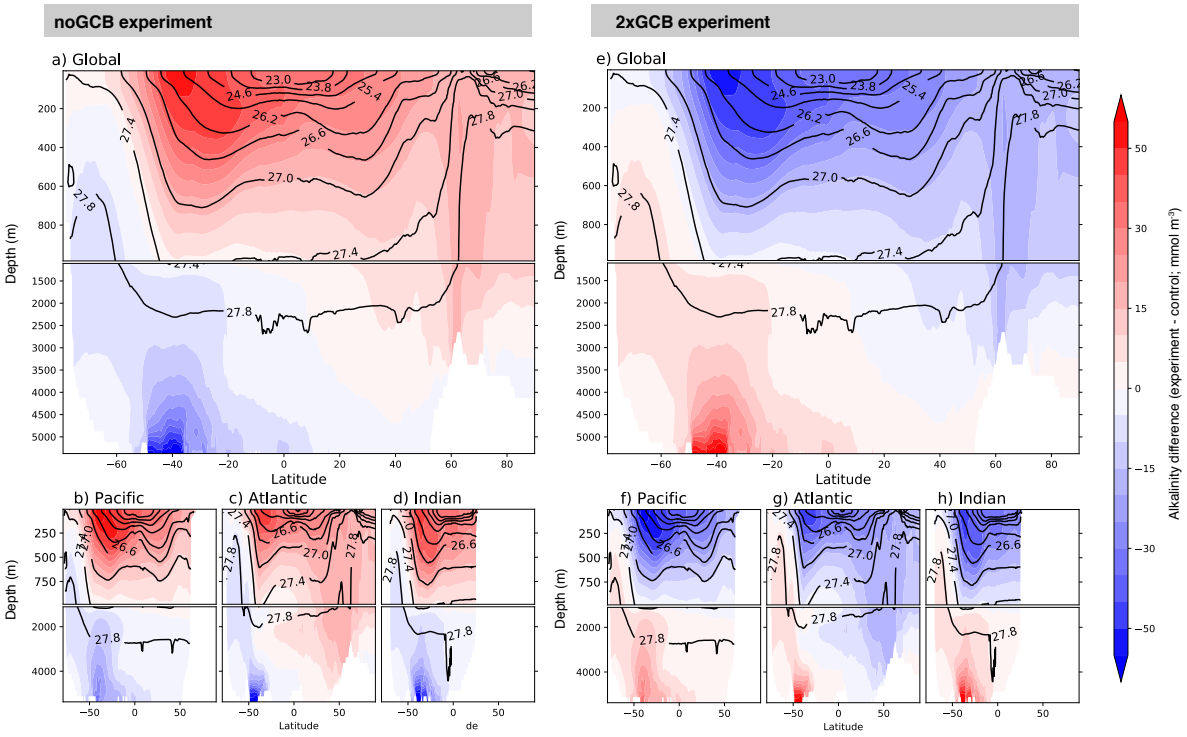

Figure 4. Zonal mean differences in alkalinity between the control and the noGBC experiment (panels a-d) and the 2xGBC experiment (panels e-h). Global zonal mean alkalinity differences are shown on top in the larger plots and the smaller plots show zonal mean differences within the Pacific, Atlantic, and Indian basins. Isopycnal layers in σ_θ coordinates are shown by contour lines. All data are averaged over the fifth IAF cycle (simulation years 249–310).

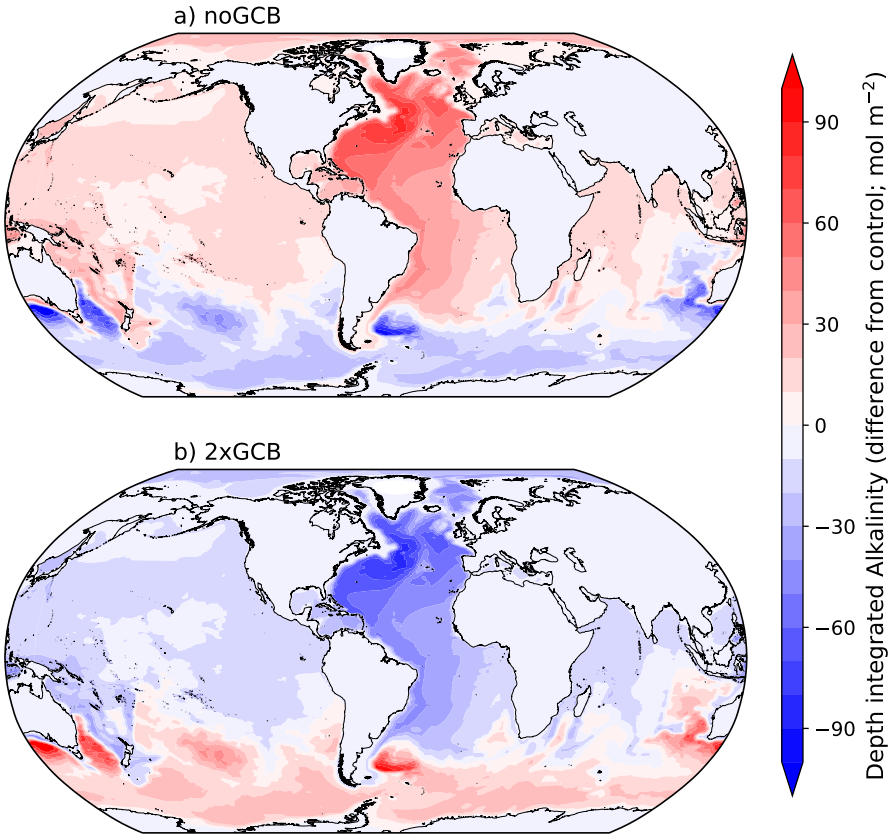

Figure 5. Horizontal shifts in depth-integrated alkalinity inventory. Panel (a) shows the difference between the noGCB experiment and the control and panel (b) shows the 2xGCB experiment difference from the control. All data are averaged over the fifth CORE-IAF cycle (simulation years 249–310).

PIC and depositing it in the deeper layers of the SAZ via carbonate dissolution. These water masses feed into the upwelling at the Antarctic divergence, thus enabling the alkalinity trapping mechanism to operate effectively. In the noGCB experiment, this vertical transfer of alkalinity is eliminated, and alkalinity escapes the Southern Ocean trap; in the 2xGBC experiments, by contrast, a greater transfer of alkalinity to the deep ocean increases the efficacy of the alkalinity trap. These processes form a critical control on the distribution of alkalinity globally.

3.4 Impacts of Southern Ocean calcification on the ocean carbon inventory

Changes in Southern Ocean calcification result in widespread changes in air-sea CO_2 fluxes. The CESM simulations were forced with a constant atmospheric CO_2 of 284.7 ppm, representative of preindustrial conditions. This fixed atmospheric boundary condition effectively makes the atmosphere an infinite CO_2 reservoir. Under such a constant atmospheric boundary condition, the control simulation would be expected to equilibrate to near-zero air-sea CO_2 flux; however, the timescale to achieve such equilibrium is much longer than our 310-year-long integrations (e.g., Lindsay et al., 2014). Moreover, a balanced DIC inventory requires riverine inputs, burial, and air-sea fluxes to sum to zero—thus the persistent drift in $CaCO_3$ burial, discussed above in the context of the alkalinity balance, also impacts the DIC inventory. As a result of this drift, we cannot definitively quantify the changes in equilibrium DIC inventory across our experiments. Our results are nevertheless informative in a qualitative sense, specifically highlighting the key role that Southern Ocean calcification plays in setting this inventory. The sensitivity experiments show significant differences in air-sea CO_2 fluxes that are indicative of the differences we expect with fully equilibrated DIC inventories.

Over the last (fifth) CORE-IAF cycle, the control had a mean oceanic CO_2 uptake of -0.14 Pg C yr^{-1} (Table 1). Shutting off Southern Ocean calcification (noGCB) resulted in a strong increase in this CO_2 uptake (-0.24 Pg C yr^{-1}), while doubling calcification brought the air-sea flux to near-zero (-0.04 Pg C yr^{-1}; Table 1). These patterns are consistent with the large-scale transfer of alkalinity to the upper ocean in noGCB, but also involve the direct impacts of calcification on DIC itself. Increasing surface alkalinity enhances the buffer capacity, effectively increasing the ocean's capacity to absorb and store CO_2. The geographical distribution of changes in air-sea CO_2 flux shows dramatically enhanced uptake in the Subantarctic in the noGCB experiments, accompanied outgassing in the Antarctic zone of the Southern Ocean (Figure 6a). This dichotomy in air-sea CO_2 flux response in the Southern Ocean is reflected in the Revelle factor (Figure S5); indeed, it is this increase in buffer capacity that drives enhanced uptake in the Subantarctic and also in the high-latitude northern hemisphere ocean in the noGCB run. While buffer capacity also increases in tropical waters in noGCB, these regions display weak anomalous outgassing relative to the control. This reflects the fact that shutting off calcification in the SAZ eliminates a sink for DIC in the upstream regions feeding tropical surface waters; therefore, more DIC flows northward to these naturally alkaline regions, driving a tendency toward CO_2 outgassing. The opposite patterns are evident in the 2xGCB (Figure 6b).

The response of air-sea flux in our sensitivity experiments is consistent with the literature examining the effect of the rain ratio on atmosphere-ocean partitioning of CO_2 over geological timescales (e.g., Matsumoto et al., 2002). While our experiments only manipulated the rain ratio south of 30°S (Figure S6), these changes have significant impacts on the global mean rain ratio (Table 1). In noGCB, for instance, the reduction in rain ratio and the response of the air-sea flux is consistent with the expectation that this simulation will equilibrate with a larger DIC inventory than the control.

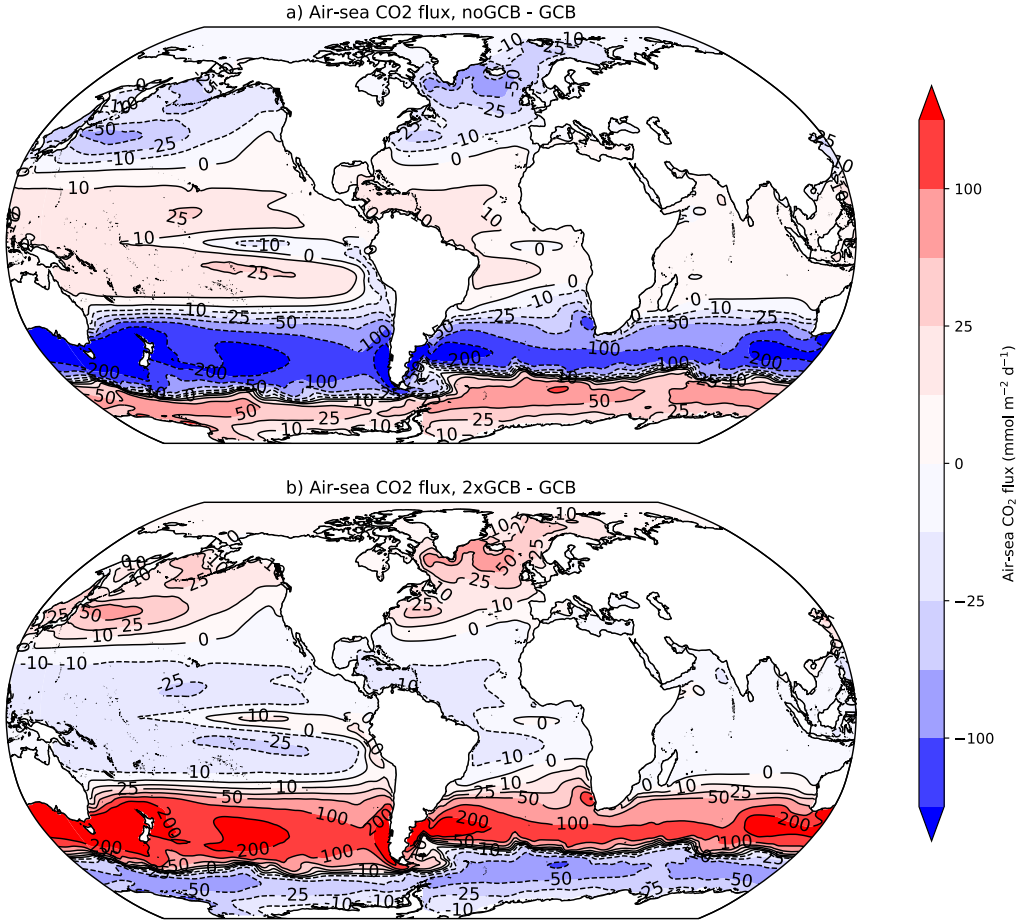

Figure 6. Changes in air-sea CO_2 flux between the control and the noGBC experiment (panels a-d) and the 2xGBC experiment, where negative (blue) values represent greater CO_2 flux into the ocean and red values represent more CO_2 fluxing out of the ocean.

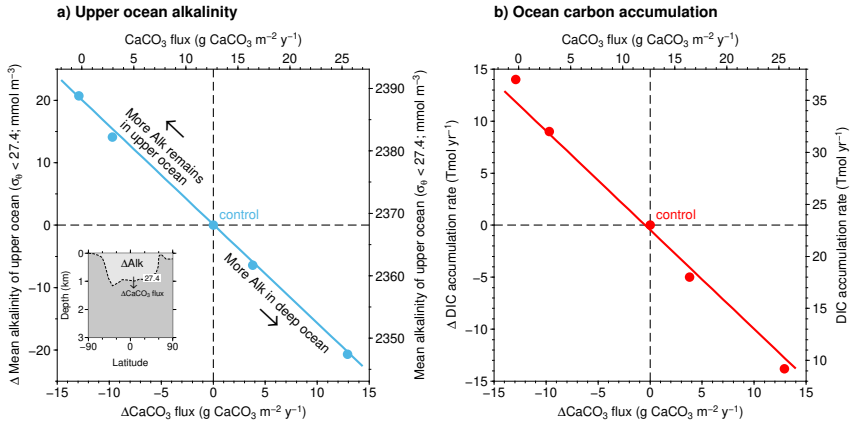

Figure 7. Mean upper ocean alkalinity (a) and DIC accumulation rates (b) as a function of GCB $CaCO_3$ fluxes across the σ_θ 27.4 isopycnal (with reference to control on left and bottom axes; absolute values shown on right and top axes). Dots are from five CESM model experiments, from left to right: noGCB, 100mDLS, control, 1000mDLS, 2xGCB (see Methods for experimental setup). The lines on each panel are from least squares linear regressions of upper ocean alkalinity and DIC accumulation rate as a function of $CaCO_3$ flux (panel a slope = -1.58 mmol m^{-3}/g $CaCO_3$ m^{-2} y^{-1}; panel b slope = -0.95 Tmol DIC yr^{-1}/g $CaCO_3$ m^{-2} y^{-1}).

3.5 Setting the Southern Ocean alkalinity trap

The Southern Ocean alkalinity trap is sustained by the vertical transfer of PIC in the Subantarctic. $CaCO_3$ production strips alkalinity out of northward flowing surface waters, depositing it at depth in the same water masses that feed Subantarctic surface waters from upwelling at the Antarctic divergence. The nature of this trapping mechanism is thus dependent on the magnitude of vertical fluxes in $CaCO_3$. To summarize this effect, we seek a relationship between the simulated alkalinity anomaly and the change in vertical $CaCO_3$ flux in the GCB region, which we define as the region below the 26.0 to 27.0 σ_θ surface outcrop (Figures 3a,b). We note that the sign of alkalinity anomalies in the noGCB and 2xGCB experiments changes around σ_θ = 27.4 (Figure 4). Therefore, we plot the change in the upper ocean alkalinity above this surface against the change in the $CaCO_3$ flux across this surface in each experiment, including those where we manipulated the dissolution length scale for sinking $CaCO_3$ (100mDLS and 1000mDLS; Figure 7a). The relationship is approximately linear and suggests that increasing the flux of $CaCO_3$ across σ_θ = 27.4 south of 30°S by 1 g $CaCO_3$ m^{-2} will reduce the mean alkalinity concentration above this surface by about 1.6 mmol m^{-3}. Thus, we may expect that variations in $CaCO_3$ fluxes in the Southern Ocean may contribute to variability in upper ocean alkalinity and thus ocean CO_2 uptake.

We further relate GCB $CaCO_3$ fluxes to ocean DIC accumulation rates (Figure 7b). The relationship between DIC accumulation in the ocean and GCB $CaCO_3$ fluxes is also approximately linear. Here, for each additional g of $CaCO_3$ crossing the 27.4 isopyncal in the ocean the ocean accumulates 0.95 Tmol C yr^{-1} less. This relationship summarizes the effect of Southern Ocean calcification on the partitioning of carbon between the atmosphere and the ocean.

4 Discussion

It has long been recognized that biological production in the Southern Ocean influences atmospheric CO_2 and global productivity via regional nutrient utilization efficiency (Knox & McElroy, 1984; Sarmiento & Orr, 1991; Ito & Follows, 2005; Marinov et al., 2006; Primeau et al., 2013). Here we have shown that biological calcification in the Southern Ocean, primarily in the GCB region, also exerts a control on global biogeochemistry by modifying the global distribution of alkalinity. Calcification and vertical $CaCO_3$ fluxes in the GCB region of the Southern Ocean lead to a net transfer of alkalinity to the deep cell of the MOC (Figure 4); this vertical flux sustains an alkalinity trap, retaining alkalinity in the Southern Ocean (Figure 5). The key constraint on this Southern Ocean alkalinity trap is the flux of $CaCO_3$ across the boundary between the upper and lower overturning cells. In CESM, this is approximately where $\sigma_\theta = 27.4$ in the GCB region of the Southern Ocean (located approximately at $\sim$1000 m for much of the ocean; Figure 4). Increasing the flux of $CaCO_3$ across this surface in the Southern Ocean strengthens the alkalinity trap, while decreasing the $CaCO_3$ flux permits more alkalinity to escape and remain in the upper ocean globally (Figure 7).

Calcification in the SAZ mixed layer depends on the organisms present and their physiological state. If coccolithophores out-compete other phytoplankton for nutrients, this could increase overall calcification. On the other hand, excess SiO_3 could lead to an increase in diatoms at the expense of coccolithophores, reducing calcification (Matsumoto et al., 2002). Since diatom-silicification rates are sensitive to iron availability, this raises the possibility that variation in iron supply might indirectly modulate calcification rates through Si drawdown patterns integrated over the Southern Ocean. More plentiful pteropods and/or foraminifera may also modulate overall calcification; their populations may be more dependent on prey availability, as well as environmental conditions (e.g., Manno et al., 2018; Meilland et al., 2016). Further, calcifying organisms may be vulnerable to ocean acidification, which may drive decreases in calcification in this naturally acidic part of the global ocean.

The Southern Ocean alkalinity trap is sensitive to the vertical distribution of $CaCO_3$ dissolution—and in particular partitioning of dissolution above and below the σ_θ 27.4 (or equivalent) isopycnal. In nature, the dissolution profile might be sensitive to biologically-mediated dissolution in microaggregates (Milliman et al., 1999). Pteropod $CaCO_3$ (in the form of aragonite) would be more susceptible to dissolution at shallow depths (Buitenhuis et al., 2019), especially if the aragonite saturation horizon shoals rapidly in the Southern Ocean, as has been projected (Negrete-García et al., 2019). The $CaCO_3$ dissolution profile is parameterized in CESM with a time-invariant dissolution length scale. The amount of deep water dissolution versus burial on the seafloor could influence the amount of alkalinity that moves south and upwells at the Antarctic divergence.

The sensitivity experiments we show here contain several important caveats and limitations. Most importantly, biases in the physical circulation of the CESM ocean component will impact the results. For example, a shallow mixed layer depth bias in the Southern Ocean affects the fidelity with which the model simulates AAIW and SAMW formation. In a previous versions of CESM, biases in mixed layer depth were linked to poor simulations of mode water and weak uptake of transient tracers, such as anthropogenic carbon and chlorofluorocarbons (Long et al., 2013; Weijer et al., 2012). While these biases may be important in controlling detailed aspects of the patterns in our results, such as the precise value of the slopes shown in Figure 7, they are not likely to impact our fundamental conclusions regarding the response of the alkalinity inventory to Southern Ocean calcification. We are confident that the model's overturning circulation is sufficiently representative of nature that these conclusions are robust. Similarly, the ocean ecosystem model is a considerable oversimplification of reality. Our 4 phytoplankton/1 zooplankton representation of ocean ecosystems ignores the intricacies and diversity present in nature. Such a simplified system usually results in one PFT dominating over the oth-

ers, rather than a more realistic, mixed plankton ecosystem. Additionally, here we only have one source of biological calcification—the coccolithophore phytoplankton functional type—and ignore distinctions between calcite and aragonite. Since aragonite is more easily dissolved in sinking material, this could be critical for the representation of shallow $CaCO_3$ dissolution and would influence how alkalinity (in the form of $CaCO_3$) sinks and is remineralized at depth (Buitenhuis et al., 2019; Manno et al., 2018; Gangstø et al., 2008). Since our primary intent, however, is to illustrate the sensitivity to imposed changes in calcification and dissolution profiles, these oversimplifications do not significantly impact our conclusions.

The sensitivity experiments we conducted are obviously highly idealized. The Southern Ocean calcification mechanism of redistributing alkalinity between the upper and lower overturning, however, may play an important role on a variety of timescales. It has long been recognized that reorganizations of phytoplankton communities over millennial timescales might influence the global rain ratio, with implications for atmosphere-ocean partitioning of CO_2 (Archer et al., 2000; Matsumoto et al., 2002). Based on our study, it is possible that the low-latitude, upper-ocean alkalinity inventory also contains decadal variability, for instance, stemming from variations in Southern Ocean calcification on these timescales. Similarly, future oceanic CO_2 uptake may include centennial-scale feedback mediated by changes in Southern Ocean calcification that alter the upper ocean's buffer capacity under transient climate change scenarios.

An additional important implication of our study is that oceanic profiles of alkalinity are not necessarily local in nature. We demonstrate this by calculating the rain ratio using the method described in Sarmiento et al. (2002), in which we compute the ratio between vertical gradients of sPAlk and salinity-normalized nitrate (nNO_3) below the mixed layer (see Figure S6). Even though calcification was only altered south of 30°S for our experiments—and thus the rain ratio was not changed outside this region—the vertical gradients in sPAlk and nNO_3 changed nearly everywhere in the ocean, and are particularly different in the southern hemisphere subtropics, the region of the thermocline most closely linked to Subantarctic surface waters. This exercise highlights the widespread impacts of Southern Ocean calcification on vertical alkalinity gradients.

5 Conclusion

In this study we demonstrate the potential of Southern Ocean calcification to alter the global distribution of ocean alkalinity. We first used sediment trap and ocean sediment data from the Southern Ocean to show that sinking $CaCO_3$ reaches depths >1000m setting up the potential for Southern Ocean alkalinity trapping; Southern Ocean $CaCO_3$ fluxes in CESM are inline with these observations (Figure 2). We identified a signature of Southern Ocean calcification in oceanic observations of alkalinity (Figure 3). We performed CESM simulations with differing Southern Ocean calcification to show that: (1) when Southern Ocean $CaCO_3$ fluxes are lessened, more alkalinity leaves in the Southern Ocean and remains in the upper cell of the MOC (Figures 4a-d, 5a); (2) when Southern Ocean $CaCO_3$ is increased, the Southern Ocean alkalinity trap is strengthened and more alkalinity is transferred to the deep ocean with relatively more alkalinity in the Southern Ocean (Figures 4e-h, 5a); and (3) changes to Southern Ocean calcification result in anomalies with respect to ocean carbon uptake and storage (Figures 6, S2). In CESM, these processes are summarized by examining $CaCO_3$ fluxes across the σ_θ 27.4 isopycnal in the GCB region of the Southern Ocean (Figure 7). The Southern Ocean alkalinity trap identified here is a novel mechanism recognized in the Earth system, relevant for paleoclimate studies as well as future projections. As calcification in the Southern Ocean continues to change due to anthropogenic climate change and ocean acidification, there could be widespread effects on global alkalinity distributions and ocean CO_2 uptake.

Acknowledgments

We are grateful for funding from the National Science Foundation (OCE-1735846). We acknowledge high-performance computing support from Cheyenne (doi:10.5065/D6RX99HX) provided by NCAR's Computational and Information Systems Laboratory, sponsored by the National Science Foundation. This material is based upon work supported by the National Center for Atmospheric Research, which is a major facility sponsored by the National Science Foundation under Cooperative Agreement No. 1852977. Data from the CESM simulations performed for this study will be made available via the DASH repository (`https://www2.cisl.ucar.edu/dash`). Analysis scripts for this project are located in a public repository on Github (`https://github.com/kristenkrumhardt/GCB_ALK_analysis`).

References

Archer, D., Winguth, A., Lea, D., & Mahowald, N. (2000). What caused the glacial/interglacial atmospheric pCO_2 cycles? *Reviews of Geophysics*, *38*(2), 159-189. Retrieved from `https://agupubs.onlinelibrary.wiley.com/doi/abs/10.1029/1999RG000066` doi: 10.1029/1999RG000066

Armstrong, R., Lee, C., Hedges, J., Honjo, S., & Wakeham, S. (2002). A new, mechanistic model for organic carbon fluxes in the ocean based on the quantitative association of POC with ballast minerals. *Deep-Sea Res.*, *49*(1–3), 219–236. doi: 10.1016/S0967-0645(01)00101-1

Assmy, P., Smetacek, V., Montresor, M., Klaas, C., Henjes, J., Strass, V. H., ... Wolf-Gladrow, D. (2013). Thick-shelled, grazer-protected diatoms decouple ocean carbon and silicon cycles in the iron-limited Antarctic Circumpolar Current. *Proceedings of the National Academy of Sciences*, *110*(51), 20633–20638. doi: 10.1073/pnas.1309345110

Balch, W. M., Bates, N. R., Lam, P. J., Twining, B. S., Rosengard, S. Z., Bowler, B. C., ... Rauschenberg, S. (2016). Factors regulating the Great Calcite Belt in the Southern Ocean and its biogeochemical significance. *Global Biogeochemical Cycles*, *30*(8), 1124–1144. (2016GB005414) doi: 10.1002/2016GB005414

Balch, W. M., Drapeau, D. T., Bowler, B. C., Lyczskowski, E., Booth, E. S., & Alley, D. (2011). The contribution of coccolithophores to the optical and inorganic carbon budgets during the Southern Ocean Gas exchange Experiment: New evidence in support of the "Great Calcite Belt" hypothesis. *Journal of Geophysical Research: Oceans*, *116*(C4). (C00F06) doi: 10.1029/2011JC006941

Balch, W. M., Gordon, H. R., Bowler, B., Drapeau, D., & Booth, E. (2005). Calcium carbonate measurements in the surface global ocean based on Moderate-Resolution Imaging Spectroradiometer data. *Journal of Geophysical Research: Oceans*, *110*(C7), 1978–2012. doi: 10.1029/2004JC002560

Bates, N. R., Michaels, A. F., & Knap, A. H. (1996). Alkalinity changes in the sargasso sea: geochemical evidence of calcification? *Marine Chemistry*, *51*(4), 347 - 358. doi: 10.1016/0304-4203(95)00068-2

Broecker, W., & Clark, E. (2009, Aug). Ratio of coccolith $CaCO_3$ to foraminifera $CaCO_3$ in late Holocene deep sea sediments. *Paleoceanography*, *24*(3). doi: 10.1029/2009pa001731

Broecker, W. S. (1991). The great ocean conveyor. *Oceanography*, *4*(2), 79–89. doi: 10.5670/oceanog.1991.07

Buitenhuis, E. T., Le Quéré, C., Bednaršek, N., & Schiebel, R. (2019). Large contribution of pteropods to shallow $CaCO_3$ export. *Global Biogeochemical Cycles*, *33*(3), 458-468. doi: 10.1029/2018GB006110

Cross, J. N., Mathis, J. T., Bates, N. R., & Byrne, R. H. (2013). Conservative and non-conservative variations of total alkalinity on the southeastern Bering Sea shelf. *Marine Chemistry*, *154*, 100 - 112. doi: https://doi.org/10.1016/

598 j.marchem.2013.05.012
599 Dutkiewicz, A., Müller, R. D., O'Callaghan, S., & Jónasson, H. (2015, 09). Census
600 of seafloor sediments in the world's ocean. *Geology*, *43*(9), 795-798. doi: 10
601 .1130/G36883.1
602 Dutkiewicz, S., Follows, M. J., & Parekh, P. (2005). Interactions of the iron and
603 phosphorus cycles: A three-dimensional model study. *Global Biogeochemical*
604 *Cycles*, *19*(1). doi: 10.1029/2004GB002342
605 Fischer, G., Gersonde, R., & Wefer, G. (2002). Organic carbon, biogenic silica and
606 diatom fluxes in the marginal winter sea-ice zone and in the polar front re-
607 gion: interannual variations and differences in composition. *Deep Sea Research*
608 *Part II: Topical Studies in Oceanography*, *49*(9), 1721 - 1745. (The Southern
609 Ocean I: Climatic Changes in the Cycle of Carbon in the Southern Ocean) doi:
610 10.1016/S0967-0645(02)00009-7
611 Franck, V. M., Brzezinski, M. A., Coale, K. H., & Nelson, D. M. (2000). Iron
612 and silicic acid concentrations regulate si uptake north and south of the polar
613 frontal zone in the pacific sector of the southern ocean. *Deep Sea Research*
614 *Part II: Topical Studies in Oceanography*, *47*(15), 3315 - 3338. (US Southern
615 Ocean JGOFS Program (AESOPS)) doi: 10.1016/S0967-0645(00)00070-9
616 Freeman, N. M., & Lovenduski, N. S. (2016). *Mapping the Antarctic Polar Front:*
617 *Weekly realizations from 2002 to 2014, links to NetCDF file and MPEG4*
618 *movie* [data set]. PANGAEA. (Supplement to: Freeman, NM; Lovenduski, NS
619 (2016): Mapping the Antarctic Polar Front: weekly realizations from 2002 to
620 2014. Earth System Science Data, 8(1), 191-198, https://doi.org/10.5194/essd-
621 8-191-2016) doi: 10.1594/PANGAEA.855640
622 Freeman, N. M., Lovenduski, N. S., Munro, D. R., Krumhardt, K. M., Lindsay, K.,
623 Long, M. C., & Maclennan, M. (2018). The Variable and Changing South-
624 ern Ocean Silicate Front: Insights From the CESM Large Ensemble. *Global*
625 *Biogeochemical Cycles*, *32*(5), 752-768. doi: 10.1029/2017GB005816
626 Fry, C. H., Tyrrell, T., Hain, M. P., Bates, N. R., & Achterberg, E. P. (2015). Anal-
627 ysis of global surface ocean alkalinity to determine controlling processes. *Ma-*
628 *rine Chemistry*, *174*, 46 - 57. doi: 10.1016/j.marchem.2015.05.003
629 Gangstø, R., Gehlen, M., Schneider, B., Bopp, L., Aumont, O., & Joos, F. (2008).
630 Modeling the marine aragonite cycle: changes under rising carbon dioxide and
631 its role in shallow water $CaCO_3$ dissolution. *Biogeosciences*, *5*(4), 1057–1072.
632 doi: 10.5194/bg-5-1057-2008
633 Gordon, H. R., Boynton, G. C., Balch, W. M., Groom, S. B., Harbour, D. S., &
634 Smyth, T. J. (2001). Retrieval of coccolithophore calcite concentration from
635 SeaWiFS imagery. *Geophysical Research Letters*, *28*(8), 1587–1590. doi:
636 10.1029/2000GL012025
637 Holligan, P., Charalampopoulou, A., & Hutson, R. (2010). Seasonal distributions of
638 the coccolithophore, Emiliania huxleyi, and of particulate inorganic carbon in
639 surface waters of the Scotia Sea. *Journal of Marine Systems*, *82*(4), 195 - 205.
640 doi: 10.1016/j.jmarsys.2010.05.007
641 Holligan, P., Fernández, E., Aiken, J., Balch, W. M., Boyd, P., Burkill, P. H., ...
642 van der Wal, P. (1993). A biogeochemical study of the coccolithophore,
643 Emiliania huxleyi, in the North Atlantic. *Global Biogeochemical Cycles*, *7*(4),
644 879-900. doi: 10.1029/93GB01731
645 Honjo, S., Francois, R., Manganini, S., Dymond, J., & Collier, R. (2000). Parti-
646 cle fluxes to the interior of the Southern Ocean in the Western Pacific sector
647 along 170 °W. *Deep Sea Research Part II: Topical Studies in Oceanography*,
648 *47*(15), 3521 - 3548. (US Southern Ocean JGOFS Program (AESOPS)) doi:
649 10.1016/S0967-0645(00)00077-1
650 Hunt, B., Pakhomov, E., Hosie, G., Siegel, V., Ward, P., & Bernard, K. (2008).
651 Pteropods in Southern Ocean ecosystems. *Progress in Oceanography*, *78*(3),
652 193 - 221. doi: 10.1016/j.pocean.2008.06.001

Ito, T., & Follows, M. (2005). Preformed phosphate, soft tissue pump and atmospheric CO_2. *Journal of Marine Research*, *63*(4), 813–839.

Jin, X., Gruber, N., Dunne, J. P., Sarmiento, J. L., & Armstrong, R. A. (2006). Diagnosing the contribution of phytoplankton functional groups to the production and export of particulate organic carbon, $CaCO_3$, and opal from global nutrient and alkalinity distributions. *Global Biogeochemical Cycles*, *20*(2). (GB2015) doi: 10.1029/2005GB002532

Knox, F., & McElroy, M. B. (1984). Changes in atmospheric CO_2: Influence of the marine biota at high latitude. *Journal of Geophysical Research: Atmospheres*, *89*(D3), 4629-4637. doi: 10.1029/JD089iD03p04629

Krumhardt, K. M., Lovenduski, N. S., Long, M. C., Levy, M., Lindsay, K., Moore, J. K., & Nissen, C. (2019, Mar). Coccolithophore growth and calcification in an acidified ocean: Insights from community earth system model simulations. *Journal of Advances in Modeling Earth Systems*. doi: 10.1029/2018ms001483

Large, W. G., & Yeager, S. G. (2009). The global climatology of an interannually varying air–sea flux data set. *Climate Dynamics*, *33*(2-3), 341–364. doi: 10.1007/s00382-008-0441-3

Lauvset, S. K., Key, R. M., Olsen, A., van Heuven, S., Velo, A., Lin, X., ... Watelet, S. (2016). A new global interior ocean mapped climatology: the 1°x1° GLODAP version 2. *Earth System Science Data*, *8*, 325–340. doi: 10.5194/essd-8-325-2016

Ledwell, J. R., Watson, A. J., & Law, C. S. (1993). Evidence for slow mixing across the pycnocline from an open-ocean tracer-release experiment. *Nature*, *364*, 701-703. doi: 10.1038/364701a0

Levitus, S., Conkright, M. E., Reid, J. L., Najjar, R. G., & Mantyla, A. (1993). Distribution of nitrate, phosphate and silicate in the world oceans. *Progress in Oceanography*, *31*(3), 245 - 273. doi: https://doi.org/10.1016/0079-6611(93)90003-V

Leynaert, A., Bucciarelli, E., Claquin, P., Dugdale, R. C., Martin-Jézéquel, V., Pondaven, P., & Ragueneau, O. (2004). Effect of iron deficiency on diatom cell size and silicic acid uptake kinetics. *Limnology and Oceanography*, *49*(4), 1134-1143. doi: 10.4319/lo.2004.49.4.1134

Lindsay, K., Bonan, G., Doney, S. C., Hoffman, F., Lawrence, D. M., Long, M. C., ... Thornton, P. E. (2014). Preindustrial Control and 20th Century Experiments with the Earth System Model CESM1(BGC). *Journal of Climate*, *27*(24), 8981-9005. doi: 10.1175/JCLI-D-12-00565.1

Long, M. C., Lindsay, K., Peacock, S., Moore, J. K., & Doney, S. C. (2013). Twentieth-Century Oceanic Carbon Uptake and Storage in CESM1(BGC). *J. Clim.*, *26*(18), 6775-6800. doi: 10.1175/JCLI-D-12-00184.1

Malinverno, E., Maffioli, P., & Gariboldi, K. (2016). Latitudinal distribution of extant fossilizable phytoplankton in the Southern Ocean: Planktonic provinces, hydrographic fronts and palaeoecological perspectives. *Marine Micropaleontology*, *123*, 41 - 58. doi: https://doi.org/10.1016/j.marmicro.2016.01.001

Manno, C., Giglio, F., Stowasser, G., Fielding, S., Enderlein, P., & Tarling, G. A. (2018). Threatened species drive the strength of the carbonate pump in the northern Scotia Sea. *Nature Communications*, *9*(1), 4592. doi: 10.1038/s41467-018-07088-y

Marinov, I., Gnanadesikan, A., Toggweiler, J. R., & Sarmiento, J. L. (2006). The Southern Ocean biogeochemical divide. *Nature*, *441*(7096), 964–967. doi: 10.1038/nature04883

Matsumoto, K., Sarmiento, J. L., & Brzezinski, M. A. (2002). Silicic acid leakage from the southern ocean: A possible explanation for glacial atmospheric pCO_2. *Global Biogeochemical Cycles*, *16*(3), 5-1-5-23. doi: 10.1029/2001GB001442

Mayorga, E., Seitzinger, S. P., Harrison, J. A., Dumont, E., Beusen, A. H., Bouwman, A., ... Van Drecht, G. (2010). Global Nutrient Export from WaterSheds

2 (NEWS 2): Model development and implementation. *Environ. Model. Softw.*, *25*(7), 837–853. doi: 10.1016/j.envsoft.2010.01.007

Meilland, J., Fabri-Ruiz, S., Koubbi, P., Monaco, C. L., Cotte, C., Hosie, G. W., ... Howa, H. (2016). Planktonic foraminiferal biogeography in the indian sector of the southern ocean: Contribution from CPR data. *Deep Sea Research Part I: Oceanographic Research Papers*, *110*, 75 - 89. doi: https://doi.org/10.1016/j.dsr.2015.12.014

Millero, F. J., Lee, K., & Roche, M. (1998). Distribution of alkalinity in the surface waters of the major oceans. *Marine Chemistry*, *60*(1), 111 - 130. doi: https://doi.org/10.1016/S0304-4203(97)00084-4

Milliman, J., Troy, P., Balch, W., Adams, A., Li, Y.-H., & Mackenzie, F. (1999). Biologically mediated dissolution of calcium carbonate above the chemical lysocline? *Deep Sea Research Part I: Oceanographic Research Papers*, *46*(10), 1653 - 1669. doi: https://doi.org/10.1016/S0967-0637(99)00034-5

Moore, J. K., Fu, W., Primeau, F., Britten, G. L., Lindsay, K., Long, M. C., ... Randerson, J. T. (2018). Sustained climate warming drives declining marine biological productivity. *Science*, *359*(6380), 1139-1143. doi: 10.1126/science.aao6379

Negrete-García, G., Lovenduski, N. S., Hauri, C., Krumhardt, K. M., & Lauvset, S. K. (2019). Sudden emergence of a shallow aragonite saturation horizon in the Southern Ocean. *Nature Climate Change*, *9*(4), 313–317. doi: 10.1038/s41558-019-0418-8

Northcote, L. C., & Neil, H. L. (2005). Seasonal variations in foraminiferal flux in the Southern Ocean, Campbell Plateau, New Zealand. *Marine Micropaleontology*, *56*(3), 122 - 137. doi: https://doi.org/10.1016/j.marmicro.2005.05.001

Orsi, A. H., Whitworth, T., & Nowlin, W. D. (1995). On the meridional extent and fronts of the antarctic circumpolar current. *Deep Sea Research Part I: Oceanographic Research Papers*, *42*(5), 641 - 673. doi: https://doi.org/10.1016/0967-0637(95)00021-W

Primeau, F. W., Holzer, M., & DeVries, T. (2013). Southern ocean nutrient trapping and the efficiency of the biological pump. *Journal of Geophysical Research: Oceans*, *118*(5), 2547-2564. doi: 10.1002/jgrc.20181

Rembauville, M., Meilland, J., Ziveri, P., Schiebel, R., Blain, S., & Salter, I. (2016). Planktic foraminifer and coccolith contribution to carbonate export fluxes over the central Kerguelen Plateau. *Deep Sea Research Part I: Oceanographic Research Papers*, *111*, 91 - 101. doi: 10.1016/j.dsr.2016.02.017

Rigual Hernández, A. S., Trull, T. W., Nodder, S. D., Flores, J. A., Bostock, H., Abrantes, F., ... Northcote, L. C. (2020). Coccolithophore biodiversity controls carbonate export in the Southern Ocean. *Biogeosciences*, *17*(1), 245–263. doi: 10.5194/bg-17-245-2020

Rigual Hernández, A. S., Flores, J. A., Sierro, F. J., Fuertes, M. A., Cros, L., & Trull, T. W. (2018). Coccolithophore populations and their contribution to carbonate export during an annual cycle in the Australian sector of the Antarctic zone. *Biogeosciences*, *15*(6), 1843–1862. doi: 10.5194/bg-15-1843-2018

Robertson, J., Robinson, C., Turner, D., Holligan, P., Watson, A., Boyd, P., ... Finch, M. (1994). The impact of a coccolithophore bloom on oceanic carbon uptake in the northeast Atlantic during summer 1991. *Deep Sea Research Part I: Oceanographic Research Papers*, *41*(2), 297 - 314. doi: 10.1016/0967-0637(94)90005-1

Salter, I., Schiebel, R., Ziveri, P., Movellan, A., Lampitt, R., & Wolff, G. A. (2014). Carbonate counter pump stimulated by natural iron fertilization in the polar frontal zone. *Nature Geoscience*, *7*(12), 885–889. doi: 10.1038/ngeo2285

Sarmiento, J. L., Dunne, J., Gnanadesikan, A., Key, R. M., Matsumoto, K., & Slater, R. (2002). A new estimate of the $CaCO_3$ to organic carbon ex-

port ratio. *Global Biogeochemical Cycles*, *16*(4), 54-1–54-12. (1107) doi: 10.1029/2002GB001919

Sarmiento, J. L., & Gruber, N. (2006). *Ocean biogeochemical dynamics*. Princeton University Press.

Sarmiento, J. L., Gruber, N., Brzezinski, M. A., & Dunne, J. P. (2004). High-latitude controls of thermocline nutrients and low latitude biological productivity. *Nature*, *427*(6969), 56–60. doi: 10.1038/nature02127

Sarmiento, J. L., & Orr, J. C. (1991). Three-dimensional simulations of the impact of Southern Ocean nutrient depletion on atmospheric CO_2 and ocean chemistry. *Limnology and Oceanography*, *36*(8), 1928-1950. doi: 10.4319/lo.1991.36.8.1928

Sarmiento, J. L., Simeon, J., Gnanadesikan, A., Gruber, N., Key, R. M., & Schlitzer, R. (2007). Deep ocean biogeochemistry of silicic acid and nitrate. *Global Biogeochemical Cycles*, *21*(1). doi: 10.1029/2006GB002720

Sigman, D. M., Hain, M. P., & Haug, G. H. (2010). The polar ocean and glacial cycles in atmospheric CO_2 concentration. *Nature*, *466*(7302), 47–55.

Smith, H. E. K., Poulton, A. J., Garley, R., Hopkins, J., Lubelczyk, L. C., Drapeau, D. T., ... Balch, W. M. (2017). The influence of environmental variability on the biogeography of coccolithophores and diatoms in the great calcite belt. *Biogeosciences*, *14*(21), 4905–4925. doi: 10.5194/bg-14-4905-2017

Takeda, S. (1998, Jun). Influence of iron availability on nutrient consumption ratio of diatoms in oceanic waters. *Nature*, *393*(6687), 774–777. doi: 10.1038/31674

Talley, L. D., Reid, J. L., & Robbins, P. E. (2003). Data-based meridional overturning streamfunctions for the global ocean. *J. Clim.*, *16*(19), 3213–3226. doi: 10.1175/1520-0442(2003)016⟨3213:DMOSFT⟩2.0.CO;2

Tréguer, P., Bowler, C., Moriceau, B., Dutkiewicz, S., Gehlen, M., Aumont, O., ... Pondaven, P. (2018). Influence of diatom diversity on the ocean biological carbon pump. *Nature Geoscience*, *11*(1), 27–37. doi: 10.1038/s41561-017-0028-x

Trull, T. W., Bray, S. G., Manganini, S. J., Honjo, S., & François, R. (2001). Moored sediment trap measurements of carbon export in the Subantarctic and Polar Frontal zones of the Southern Ocean, south of Australia. *Journal of Geophysical Research: Oceans*, *106*(C12), 31489-31509. doi: 10.1029/2000JC000308

Trull, T. W., Passmore, A., Davies, D. M., Smit, T., Berry, K., & Tilbrook, B. (2018). Distribution of planktonic biogenic carbonate organisms in the southern ocean south of australia: a baseline for ocean acidification impact assessment. *Biogeosciences*, *15*(1), 31–49. doi: 10.5194/bg-15-31-2018

Wefer, G., & Fischer, G. (1991). Annual primary production and export flux in the Southern Ocean from sediment trap data. *Marine Chemistry*, *35*(1), 597 - 613. doi: 10.1016/S0304-4203(09)90045-7

Weijer, W., Sloyan, B. M., Maltrud, M. E., Jeffery, N., Hecht, M. W., Hartin, C. A., ... Landrum, L. (2012). The Southern Ocean and Its Climate in CCSM4. *Journal of Climate*, *25*(8), 2652-2675. doi: 10.1175/JCLI-D-11-00302.1

Wilks, J. V., Rigual-Hernández, A. S., Trull, T. W., Bray, S. G., Flores, J.-A., & Armand, L. K. (2017). Biogeochemical flux and phytoplankton succession: A year-long sediment trap record in the australian sector of the subantarctic zone. *Deep Sea Research Part I: Oceanographic Research Papers*, *121*, 143 - 159. doi: 10.1016/j.dsr.2017.01.001

Wolf-Gladrow, D. A., Zeebe, R. E., Klaas, C., Körtzinger, A., & Dickson, A. G. (2007). Total alkalinity: The explicit conservative expression and its application to biogeochemical processes. *Marine Chemistry*, *106*(1), 287 - 300. (Special issue: Dedicated to the memory of Professor Roland Wollast) doi: https://doi.org/10.1016/j.marchem.2007.01.006

Yeager, S. G., Danabasoglu, G., Rosenbloom, N., Strand, W., Bates, S., Meehl,

G., ... et al. (2018). Predicting near-term changes in the Earth System: A large ensemble of initialized decadal prediction simulations using the Community Earth System Model. *Bull. Amer. Meteor. Soc.*. doi: 10.1175/bams-d-17-0098.1

Supporting Information for "Southern Ocean calcification controls the global distribution of alkalinity"

K. M. Krumhardt[1], M. C. Long[1], K. Lindsay[1], M. Levy[1]

[1]Climate and Global Dynamics, National Center for Atmospheric Research, Boulder, Colorado, U.S.A.

Contents of this file

1. Figures S1 to S6

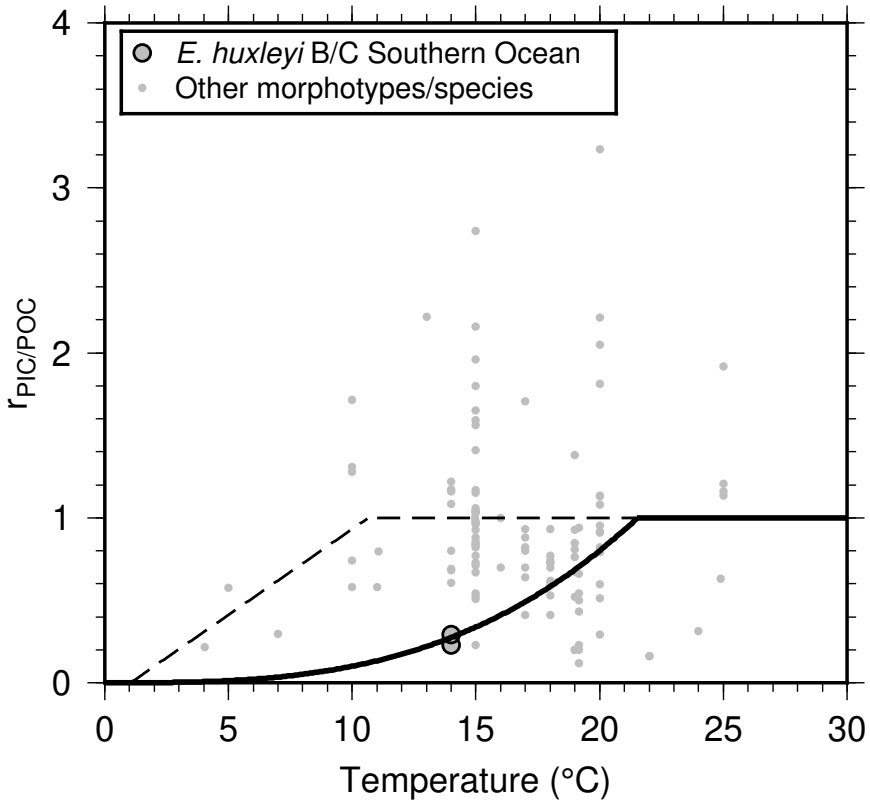

Figure S1. Refined particulate inorganic carbon (PIC) to particulate organic carbon (POC) production ratio in coccolithophore growth in CESM2 with coccolithophores. The new relationship is shown by the solid black line, while the relationship used previously (Krumhardt et al., 2019) is shown by the dashed line. Data points from experiments with the Southern Ocean *Emiliania huxleyi* morphotype are enlarged and outlined with black circles.

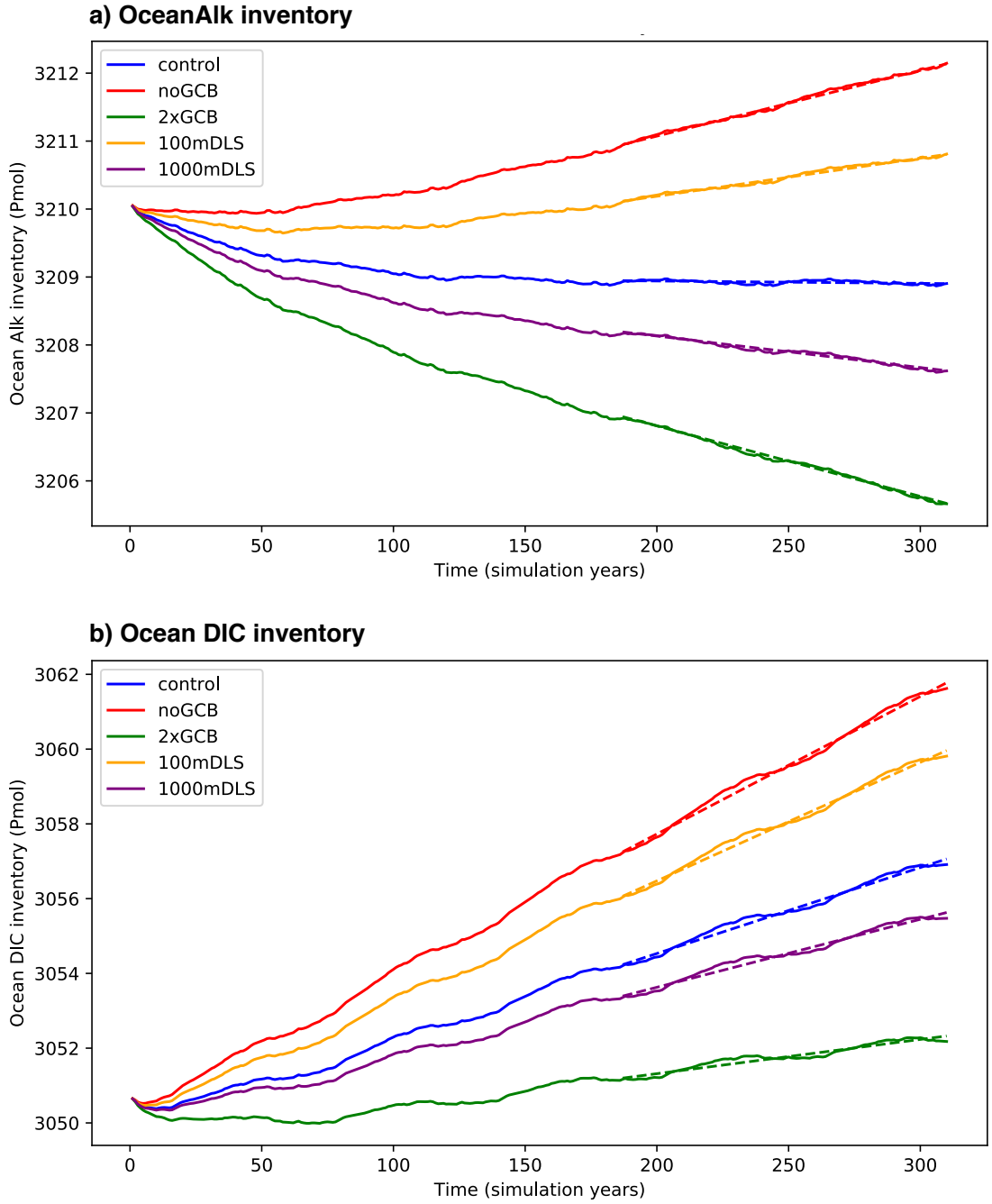

Figure S2. Ocean Alkalinity (Alk; panel a) and dissolved inorganic carbon (DIC; panel b) inventory time-series over the course of each experiment and the control. Least-squares regression lines were computed over the last two interannual forcing cycles (124 years), shown here in dashed lines. The slopes of these lines (Alk and DIC accumulation rates) are reported in Table 1.

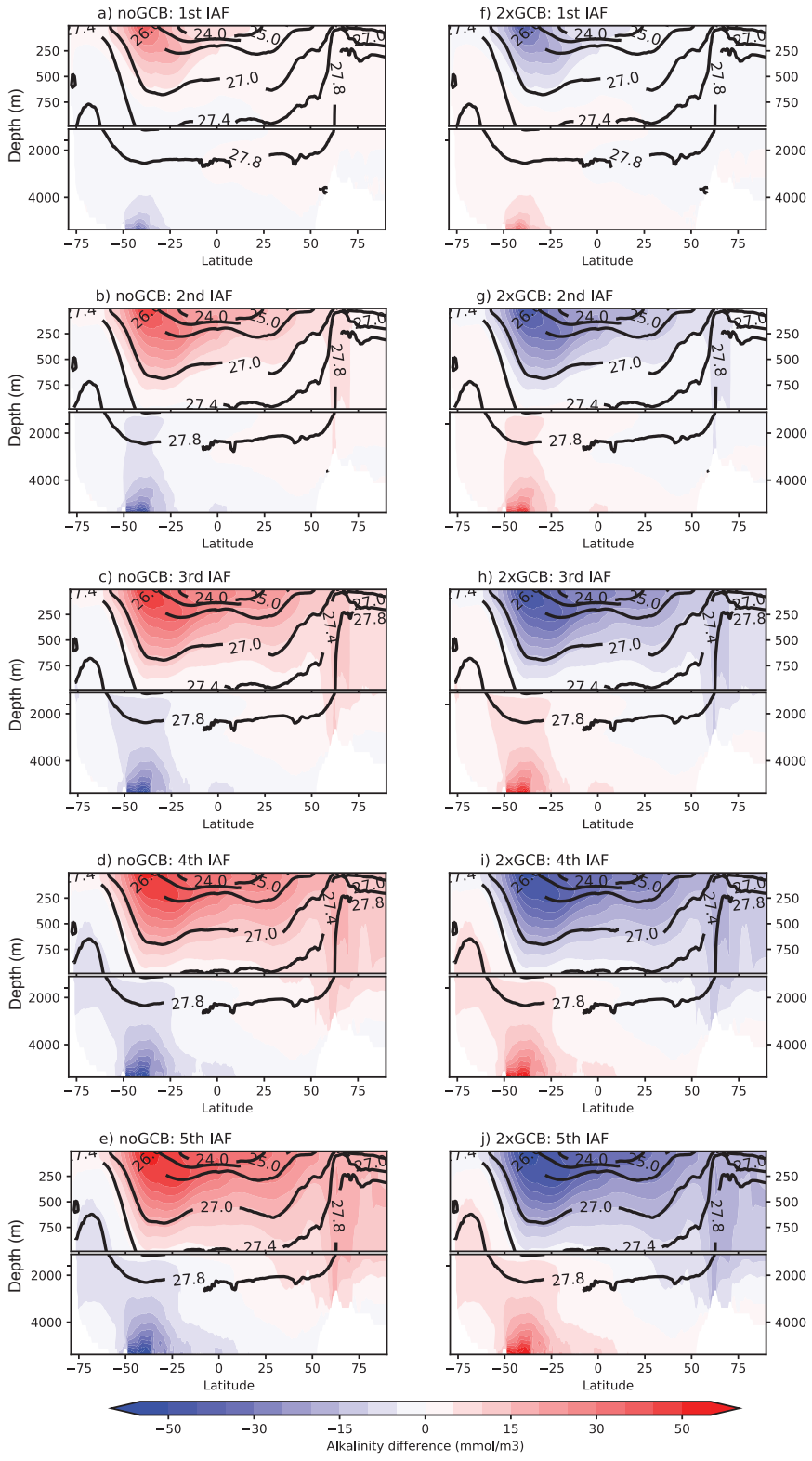

Figure S3. Zonal global mean differences in alkalinity between the control and the noGBC experiment (panels a-e) and the 2xGBC experiment (panels f-j). Each row is representative of a mean zonal difference for each interannual forcing (IAF) cycle (62 years/cycle), with the first IAF cycle on the top row and the fifth on the bottom. Isopycnal layers in σ_θ coordinates are

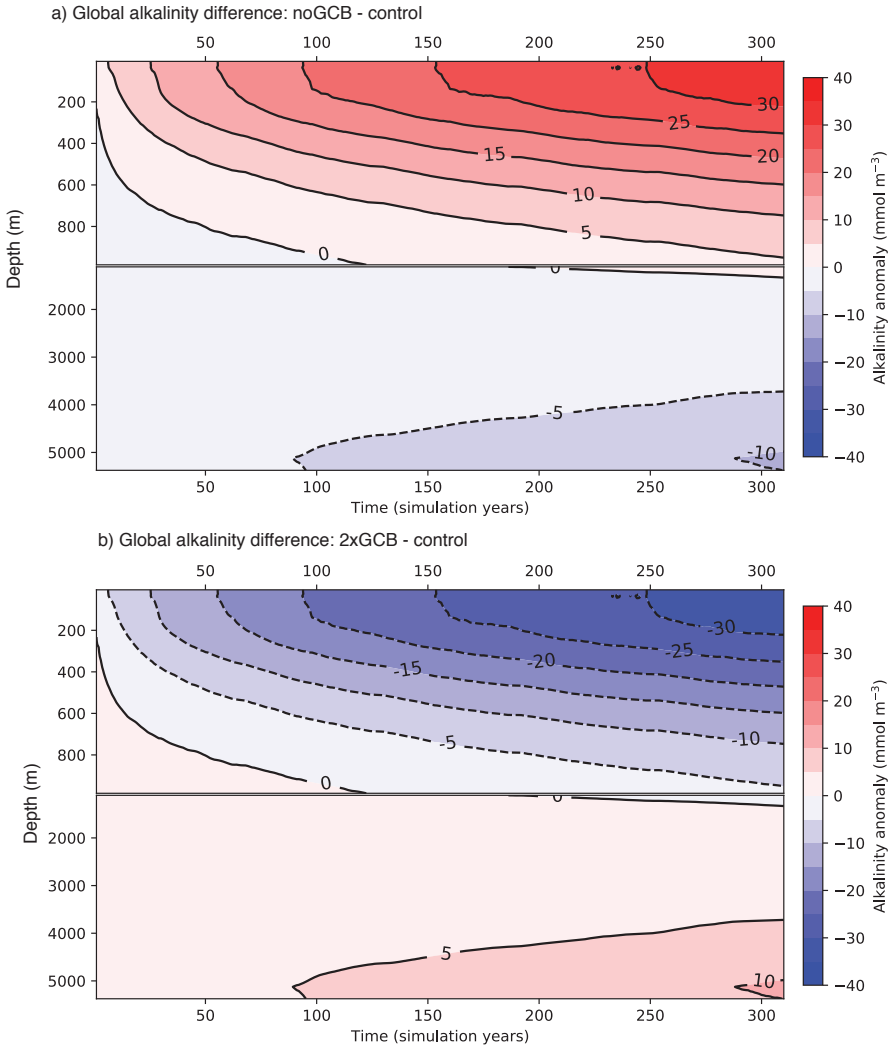

Figure S4. Global mean Hovmöller diagrams of alkalinity anomalies for the noGCB (a) and 2xGCB (b) experiments. Panels show alkalinity differences from the control in a depth versus time field for our 310-year CESM integrations. Note the explanded top 1000m depth axis.

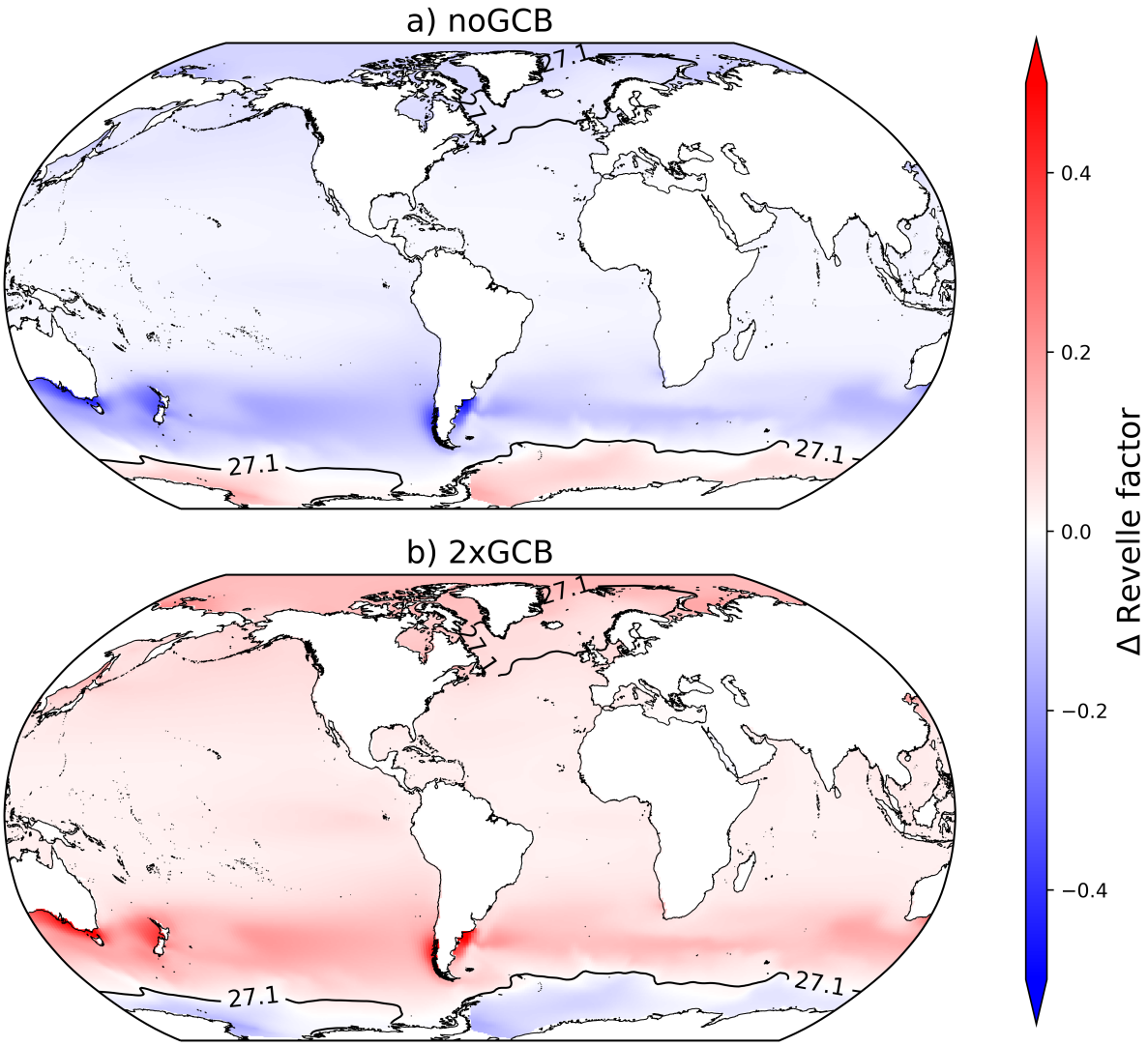

Figure S5. Changes in the Revelle factor relative to the control for the noGCB experiment (a) and the 2xGCB experiment (b).

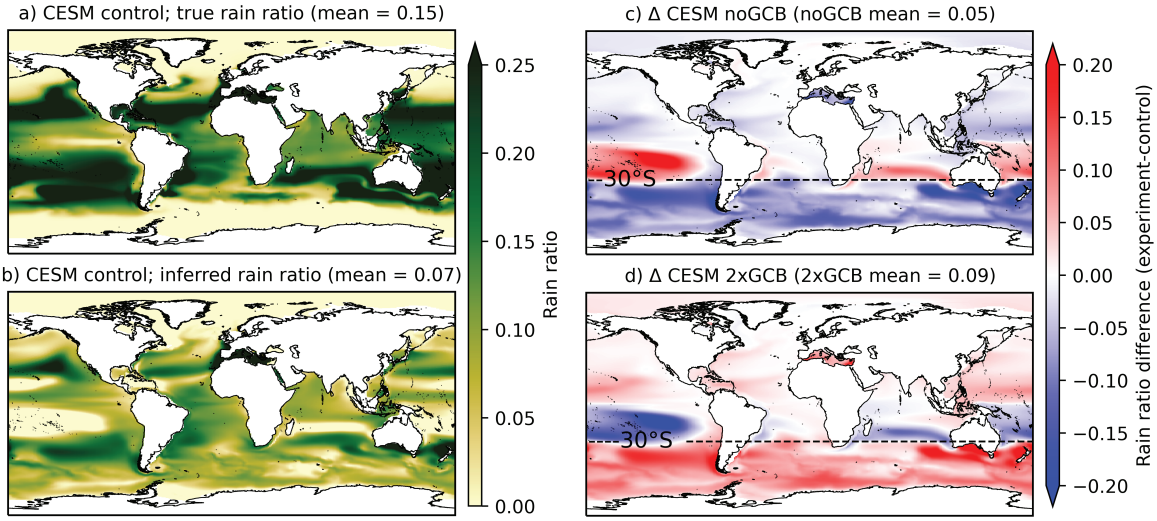

Figure S6. The true rain ratio (a) and inferred rain ratio (calculated as in Sarmiento et al., 2002) for the CESM control simulation, and changes in the inferred rain ratio for the noGCB (c) and 2xGCB (d) experiments, with reference to the control. The true rain ratio is the ratio of $CaCO_3$ flux and particulate organic carbon flux at 100 m. The inferred rain ratio is based on vertical gradients of salinity-normalized potential alkalinity and salinity-normalized nitrate (Sarmiento et al., 2002).